The carnivoran adaptive landscape reveals functional trade-offs among the skull, appendicular, and axial skeleton

Chris J. Law[1,2,3], Leslea J. Hlusko[4], Z. Jack Tseng[3]

[1]Department of Integrative Biology, University of California Berkeley

[2]Burke Museum and Department of Biology, University of Washington

[3]Department of Integrative Biology, University of Texas

[4]National Research Center on Human Evolution (CENIEH), Burgos, Spain

Abstract

Analyses of form-function relationships are widely used to understand links between morphology, ecology, and adaptation across macroevolutionary scales. However, few have investigated functional trade-offs and covariance within and between the skull, limbs, and vertebral column simultaneously. In this study, we investigated the adaptive landscape of skeletal form and function in carnivorans to test how functional trade-offs between these skeletal regions contribute to ecological adaptations and the topology of the landscape. We found that morphological proxies of function derived from carnivoran skeletal regions exhibit trade-offs and covariation across their performance surfaces, particularly in the appendicular and axial skeletons. These functional trade-offs and covariation correspond as adaptations to different adaptive landscapes when optimized by various factors including phylogeny, dietary ecology, and, in particular, locomotor mode. Lastly, we found that the topologies of the optimized adaptive landscapes and underlying performance surfaces are largely characterized as smooth, gradual gradients between regions of low and high adaptive zones rather than as rugged,

multipeak landscapes. Our results suggest that carnivorans may already occupy a broad adaptive zone as part of a larger mammalian adaptive landscape that masks the form and function relationships of skeletal traits.

Key words: Adaptive peak, Carnivora, ecomorphology, functional morphology, phylogenetic comparative methods

Introduction

The diversity of animal forms is one of the most salient patterns across the tree of life, and how morphological variation relates to the ecological diversity and survival of species across macroevolutionary time remains a core question in evolutionary biology. The varying strength of form–function relationships provide biologists with insight into the specificity of morphological structure in determining species' abilities to carry out ecological tasks (i.e., performances), especially when behavioral observations are scarce. Thus, performance is considered the link between morphology, ecology, and fitness [1–3]. Functional traits (i.e., morphological, phenological, and physiological traits affecting fitness) are often used to estimate performance [3]. Although many studies have examined the form-function relationship of the skull [4–7], appendicular skeleton [8–11], and axial skeleton [12–16], few have investigated functional trade-offs and covariation among these three major skeletal systems.

The rise of adaptive landscape analyses enables researchers to investigate the adaptive evolution of performance by elucidating the underlying links among morphology, ecology, and fitness benefits (i.e., adaptiveness) at the macroevolutionary level [17]. Ornstein–Uhlenbeck (OU) models [18–22] are widely used to test for the presence of adaptive zones or peaks (e.g., [7,23–28]). However, it remains difficult to characterize the full topology (i.e., peaks, valleys,

and slope) of the adaptive landscape as well as assess the relative importance of multiple performance traits and their contributions to overall adaptive fitness using these models. Adaptive landscape analyses [11,15,29] can overcome these limitations by examining the distribution of species in morphospace and its relationship to the relative importance of various functional traits on the topology of the adaptive landscape. Nevertheless, while an increasing number of studies have used functional adaptive landscapes to examine links between morphological diversity and functional performance [6,11,13,15,16,29], no study has yet to investigate functional trade-offs and covariation among the skull, limbs, and vertebral column.

Here, we investigate the adaptive landscape of skeletal form and function in carnivoran mammals to test how functional trade-offs contribute to ecological adaptations and landscape topology. We use carnivorans (e.g., bears, cats, dogs, seals, and their relatives) as our model system to examine the evolution of skeletal form and function because of their high species richness and broad morphological and ecological diversity. Numerous studies have investigated the morphological diversity of the carnivoran skull [4,30–35], appendicular skeleton [36–41], vertebral column [42–44], and overall body plan [23,45,46]. This diversity is attributed to mosaic evolution, in which different skeletal components exhibit distinct modes of evolution either from phylogenetic natural history [47] or from selection for ecological adaptations [48]. The ability of individual skeletal components to adapt to specific ecological factors independently from each other may have contributed to the clade's hierarchical evolution. The hierarchical evolution is primarily framed by dental adaptations along an axis of dietary resource use, which are hypothesized to facilitate the early radiation of carnivorans across a rugged, multi-peak adaptive landscape [33]. Subsequent evolution led to the continual partitioning between clades, resulting in the origination of extant carnivoran families that occupy different adaptive zones [49] with

distinct morphologies in the skull, appendicular, and axial skeletons [34,45,48]. Skeletal variation in the mandible, hindlimb, and post-diaphragmatic region of the vertebral column then arose along shared ecological axes among taxa, theoretically leading to distinct ecological peaks across the adaptive landscape [34,48].

However, the functional implications of these skeletal traits remain to be tested across the adaptive landscape; that is, how do morphological traits in the skull, appendicular skeleton, and vertebral column dictate the ecological performance of carnivoran species? Previous work using OU modeling provided evidence that morphological proxies for appendicular function exhibit relatively low ruggedness across the adaptive landscape despite also exhibiting distinct adaptive peaks [23]. Thus, the interpretation of the ruggedness of the adaptive landscape or steepness of adaptive peaks remains difficult to ascertain using OU models and may depend on different ecological contexts as well as the use of either morphological or functional traits. In this study, we advance the investigation of the carnivoran adaptive landscape using adaptive landscape analyses to investigate the functionality of the skull, appendicular, and axial skeletons simultaneously. We assessed if performance surfaces reveal trade-offs/covariation among morphological proxies of function from the skull, appendicular, and axial skeleton and test hypotheses on how these functional proxies contribute to unique adaptive landscapes along locomotor, dietary, and phylogenetic axes. Morphological traits are often associated with locomotor and dietary adaptive peaks [23,33,34,48]. Therefore, we predicted that functional trade-offs/covariation across the performance surfaces will correspond to distinct landscape topologies that is primarily driven by specialized locomotor modes (i.e., arboreality, cursoriality, fossoriality, natatoriality) and hypercarnivory. Our examination of these adaptive landscapes provide further insight on carnivoran evolution.

Methods

Morphospace and functional proxies

We created a morphospace of 109 terrestrial carnivoran species based on 136 linear and angular measurements that capture morphological variation across the entire skeleton (Fig. S1). We were able to incorporate representatives from 12 of the 13 extant terrestrial carnivoran families; specimens from Prionodontidae were unavailable. We removed size effects on linear measurements by calculating the log shape ratio (i.e., ln[trait/size]) of each skeletal trait, where size is the geometric mean of all linear trait measurements. We used only adult male specimens because carnivorans exhibit differing degrees of sexual dimorphism [50]. We then conducted a principal component analysis (PCA) using the covariance matrix on all size-corrected measurements and used the first two PC axes (46.7% of the total variance) to create the morphospace (Fig. 1; see Table S1 for PC loadings). Carnivoran species are widely distributed across the morphospace except for the bottom-left region in which no species occupy (-PC1, -PC2).

To fully sample skeletal variation throughout the morphospace, we generated 63 theoretical species evenly across the morphospace in a 9 x 7 grid along the first two PCs. We then generated theoretical morphological traits from each of the 63 theoretical species and calculated 27 functional proxies (Table 1; see Supplementary Materials for full biomechanical and ecomorphological justification) that capture the functional diversity of the skull [51], limbs [39,52], and vertebral column [13,53,54].

Ecological traits

We classified the 109 carnivoran species into one of seven locomotor regimes associated with carnivoran foraging: arboreal, cursorial, scansorial, semi-aquatic, semi-fossorial, and terrestrial. Terrestrial species were further categorized as terrestrial hunters and terrestrial non-hunters. We also classified each species into one of seven dietary regimes: large prey hypercarnivory, medium prey hypercarnivory, small prey hypercarnivory, omnivory, insectivory, aquatic carnivory, and herbivory. Definitions for locomotor and dietary regimes were obtained from [34,45] with minor edits based on literature review. See Supplementary Materials for full definitions of each locomotor and dietary regime.

Performance surfaces and adaptive landscapes

We investigated the functional optimality of the skeleton using adaptive landscape analyses [11,13,15,29] in the R package Morphoscape [29]. We first created 27 performance surfaces by interpolating each of the 27 functional proxies across the morphospace surface using ordinary kriging. We then computed a combined adaptive landscape (W) as the summation of all 27 performance surfaces (F_n), each weighted by their relative importance or contribution to overall fitness (w_n) [15]:

$$W = w_1F_1 + w_2F_2 + \bullet\bullet\bullet + w_nF_n$$

where W is optimized as the likelihood of combinations of performance surface and relative fitness, under the definition that the total fitness sums to 1 and the variance of all surfaces is equal [15]. We tested all possible combinations of weights, ranging from 0 to 1 in increments of 0.25, across a total of 27,405 possible adaptive landscapes. We then identified the optimally weighted landscape that maximizes the fitness of each locomotor regime, and tested whether these optimal landscapes are significantly different among locomotor ecological groups by comparing the number of landscapes shared by the top 5% of each group with the total number

of landscapes in the top 5% of models [13]. We also investigated differences in adaptive landscapes among dietary groups and carnivoran families that contained more than one species.

Lastly, we conducted a series of sensitivity analyses to investigate whether (1) the coarse increments of partition weights, (2) the size of the grid used to generate theoretical species, (3) the use of functional proxies derived from theoretical species rather than from actual species, and (4) removing the effects of size on the morphological traits in creating the morphospace may potentially influence our results. We found that these factors do not affect our findings (see Sensitivity Analyses section in the Supplementary Materials).

Results

Performance surfaces reveal functional trade-offs

Each functional proxy mapped onto the morphospace revealed both unique and similar performance surfaces that characterize trait groups, suggesting that functional trade-offs and covariation are present within and among skeletal systems. In the skull, mechanical advantage of jaw closure tends to be greatest in the bottom of morphospace, with temporalis mechanical advantage (temMA) highest towards the bottom-left (-PC1, -PC2) and declining towards the top-right (+PC1, +PC2) whereas masseter mechanical advantage (masMA) is highest towards the bottom-right (+PC1, -PC2) and declines towards the top-left (-PC1, +PC2) (Fig. 2).

In the forelimb, there is a trade-off between limb elongation and elbow robustness: functional proxies of scapula (SI), radius (BI), and metacarpal (MAN) elongation are highest in the top-right (+PC1, +PC2) of morphospace and transitions towards increased robustness diagonally to the bottom-left (-PC1, -PC2). Proxies associated with increased mechanical advantage of elbow extension (OLI) and attachment sites for forearm flexor, pronator, and

supinator muscles on the humeral epicondyles (HEI) and ulna (URI) exhibit the opposite pattern (i.e., highest in the bottom-left and lowest in the top-right). Overall robustness of humerus (HRI) is highest on the left side of the morphospace (-PC1) and transitions towards increased elongation to the right (+PC1), following a similar distribution as the latter indices. The hindlimb also exhibits a trade-off between elongation and robustness: indices of tibial (CI) and metatarsal (PES) elongation tend to be highest in the right side (+PC1, with CI also trending towards -PC2) and transitions to increased robustness towards to the left side (-PC2), whereas indices for femoral (FEI, FRI) and tibial (TRI) robustness tend to be highest on the left side (-PC1) but transitions towards less robustness on PC2 (FEI and FRI is highest towards -PC2 and TRI is highest towards +PC2).

In the vertebral joints, the performance surfaces show a trade-off between joint torsional angle (JTA) as a proxy for range of rotational motion and joint verticality (JV) as a proxy for sagittal mobility. For the cervical, diaphragmatic, and lumbar joints, JTA is highest in the bottom-left of the morphospace (-PC1, -PC2) and declines diagonally to the top-right (+PC1, +PC2), whereas JV exhibits the opposite pattern (i.e., highest in the top-right and lowest in the bottom-left). The thoracic vertebra exhibits similar JTA and JV distributions but in the horizontal plane (i.e., highest JTA in the left side of morphospace and highest JV in the right). In all vertebral joints, second moment of area (SMA) as a proxy for stiffness tends to be greatest towards the top-left of morphospace (-PC1, +PC2) and declines towards the right side of morphospace (+PC1).

Optimized Adaptive Landscapes

After summation of all performance surfaces based on optimized weights, we found that the combined adaptive landscape is heavily weighted for sagittal mobility of the pre-

diaphragmatic thoracic region (w_{JV} = 0.71; Fig. 3A; Table S2). When adaptive landscapes are optimized by locomotor ecologies, we found different degrees to which the 27 functional proxies are incorporated among the different adaptive landscapes. The cursorial landscape is characterized by evenly weighted functional proxies associated with increased sagittal mobility of the vertebral column (w_{JV} = 0.13–0.20 for the cervical, pre-diaphragmatic thoracic, diaphragmatic, and lumbar regions) and lengthening of the forelimb, particularly in the scapula (w_{SI} = 0.09), radius (w_{BI} = 0.13), and metacarpal (w_{MAN} = 0.07) (Fig. 3C; Table S2). This landscape is significantly different from all other locomotor landscapes except with the terrestrial non-hunter landscape (Table 2). Semi-aquatic and semi-fossorial landscapes do not significantly differ from one another (P = 0.917; Table 2), and both are weighted for increased joint torsion in the cervical (w_{JTA} = 0.25), diaphragmatic (w_{JTA} = 0.09), and lumbar (w_{JTA} = 0.22) regions; larger femoral epicondyles (w_{FEI} = 0.25); and enlarged olecranon processes (w_{OLI} = 0.09) (Fig. 3E, F; Table S2). The remaining locomotor landscapes do not significantly differ from one another (Table 2) and are heavily weighted for sagittal mobility of the pre-diaphragmatic thoracic region (w_{JV} = 0.51–0.78; Fig. 3; Table S2).

When adaptive landscapes are optimized by dietary ecologies, we found that differences in landscapes appear associated with carnivory (Fig. S2; Table S3). Adaptive landscapes based on diets that largely consists of terrestrial vertebrate prey (i.e., carnivory and omnivory) are heavily weighted for sagittal mobility of the pre-diaphragmatic thoracic region (w_{JV} = 0.66–0.70; Fig. S2; Table S4). In contrast, adaptive landscapes based on diets that do not incorporate terrestrial vertebrate prey (i.e., herbivory, insectivory, and piscivory) are characterized by evenly weighted functional proxies associated with increased joint torsion in the cervical and lumbar regions and larger femoral epicondyles (Fig. S2; Table S4).

Lastly, we found different adaptive landscapes when they are optimized by family. Adaptive landscapes for felids, viverrids, euplerids, herpestids, and procyonids are not significantly different from each other and all remain heavily weighted for sagittal mobility of the pre-diaphragmatic thoracic region (w_{JV} = 0.52–0.79; Fig. 4; Table S5; Table S6). The canid landscape resembles the cursorial landscape with similar weights for increased sagittal mobility of the pre-diaphragmatic thoracic (w_{JV} = 0.36) and diaphragmatic (w_{JV} = 0.23) joints and lengthening of the scapula (w_{SI} = 0.14) (Fig. 4G; Table S5); however, it does not significantly differ from the above family-specific landscapes (Table S6). The mephitid and mustelid landscapes resemble semi-aquatic and semi-fossorial landscapes with similar weights for larger femoral epicondyles (w_{FEI} = 0.21–0.34) and increased joint torsion in the cervical (w_{JTA} = 0.20–0.29) and lumbar (w_{JTA} = 0.16–0.19) joints (Fig. 4I, K), but only the mephitid landscape significant differs from all other families (Table S6). The hyaenid landscape weighted heavily for increased stiffness of all the cervical joints (w_{SMA} = 0.40) and elongation of the radius (w_{BI} = 0.22) (Fig. 4D), whereas the ursid landscape weighted heavily among increased stiffness of all the vertebral joints ($\sum w_{SMA}$ = 0.53) and increased robustness of the humerus (w_{HRI} = 0.18) and tibia (w_{TRI} = 0.20) (Fig. 4H). Both hyaenid and ursid landscapes significantly differ with all other family-specific landscapes (Table S6).

Discussion

The diversity found in the carnivoran skeletal system is attributed to mosaic evolution, in which the mandible, hindlimb, and post-diaphragmatic vertebrae showed evidence of adaptation towards ecological regimes whereas the cranium, forelimb, and pre-diaphragmatic vertebrae reflect clade-specific evolutionary shift [48]. Using adaptive landscape analyses, we further found that functional proxies derived from this morphological diversity exhibit trade-offs and

covariation across their performance surfaces, particularly in the appendicular and axial skeletons. These functional trade-offs and covariation corresponded as adaptations to different adaptive landscapes when optimized by various factors including phylogeny, dietary ecology, and, in particular, locomotor mode. Lastly, these adaptive landscapes and underlying performance surfaces were characterized by rather broad slopes, hinting that carnivorans occupy a broad adaptive zone as part of a larger mammalian adaptive landscape that masks the form and function relationships of skeletal traits.

Performance surfaces reveal trade-offs among functional proxies

In the appendicular skeleton, we confirmed hypotheses that the gradient from gracility to robustness often found as the primary source of variation across limb bone morphospace [40,41,55–59] signifies a functional trade-off between increasing cost of transport associated with cursoriality and resisting stresses associated with locomoting through resistant media (Fig. 2B). Specifically, long, gracile limb bones particularly on the distal ends of the limbs facilitate increased stride length and decreased moment of inertia of limbs, which in turn decreases the energetic cost of transport and increases running speeds [60–66]. In contrast, short, robust limb bones facilitate resistance to bending and shearing stresses and increased mechanical advantage for forceful movements by reducing the out-lever of the limb and increasing the in-lever of muscle forces [67,68]. Robustness also permits increased surface area of the bone for more muscles to attach. Enlargement of the humeral and femoral epicondyles increases the attachment sites of several muscles (i.e., flexors, pronators, and supinators in the forelimb and gastrocnemius and soleus muscles in hindlimb) responsible for generating power, force, and stability [52,67,69,70]. Additionally, an enlarged olecranon process facilitates stronger extension and flexion of the elbow and wrist by increasing mechanical advantage of the triceps brachii and

dorsoepitrochlearis muscles and providing greater attachment sites for the ulnar head of the flexor carpi ulnaris [52,67,69,70]. These adaptations facilitate the ability to generate large forces during certain locomotor behaviors such as digging [39,59,67,69–71] or swimming [39,58,72,73].

In the axial skeleton, our investigation using functional proxies suggested that carnivorans exhibit trade-offs between joint mobility, range of axial rotation, and, to a lesser extent, stiffness of the vertebral column. That is, high sagittal mobility covaries with low range of axial rotation and low stiffness whereas low sagittal mobility covaries with high range of axial rotation and high stiffness. This pattern was surprising because, compared to other tetrapods, mammals exhibit intervertebral joints that are characterized by high sagittal mobility, high axial rotation, and high stiffness [13]. A possible explanation was that the covariation between high sagittal mobility and low axial rotation may serve as a further adaptation to increasing forward locomotion by prioritizing flexibility in the sagittal plane through the reduction of torsional twisting. High mobility of the backbone in the sagittal plane has long been recognized as a key adaptation facilitating the diversity of different locomotor habits in mammals, particularly asymmetrical gaits (e.g., gallop, half-bound, bound) by enabling extensive dorsoventral flexion of the body axis [74–77]. The reduction of torsional twisting in carnivorans may, therefore, prioritize force generation in the sagittal plane (rather than parasagittal or transverse plane) needed for these locomotor behaviors. Evidence for this hypothesis was found in comparisons with ungulates, where carnivorans exhibit up to ~38° more sagittal mobility in the lumbar region and up to 200% less axial rotational mobility in the thoracic region compared to ungulates [78–80]. Increased rotational mobility of the backbone in ungulates is hypothesized to enhance agile

maneuvering such as sharp cornering and quick directional changes when escaping from predators [80].

Our investigation with functional proxies also suggested that high sagittal mobility loosely covaries with low stiffness of the intervertebral joints, a surprising result considering that stiffness is often hypothesized to help store elastic energy in the back between strides [13,53,81,82]. A possible explanation was that the aponeurosis of the longissimus dorsi muscle and paravertebral muscles serve as more important storage for elastic energy than the backbone [81,83,84]. Alternatively, as mammals [13], carnivorans already exhibit optimally stiff backbones that are sufficient for elastic energy storage for their range of locomotor behaviors. Therefore, selection has not led to increased stiffness, and the majority of carnivorans are distributed close to the valley of the performance surface. Earlier work indicates that carnivorans exhibit lower intervertebral joint stiffness compared to a crab-eating macaque and red-necked wallaby [85], two species with specialized forms of locomotion not found in carnivorans. Thus, additional work is needed to understand how the stiffness of intervertebral joints in carnivorans compare with other mammals.

Functional covariation between appendicular and axial skeletons optimizes the adaptive landscapes of some locomotor ecologies

The optimized adaptive landscape is heavily weighted for sagittal mobility of the pre-diaphragmatic thoracic joints (Fig. 3A), indicating that flexibility in the sagittal plane serves an important functional role for all carnivorans. When the adaptive landscapes are optimized based on locomotor ecology, we found that only cursorial, semi-aquatic, and semi-fossorial landscapes were significantly different (Fig. 3; Table 2). Correspondingly, the functional trade-offs

identified by the performance surfaces are associated with these three locomotor modes, with cursoriality on one end and semi-aquatic and semi-fossorial behaviors, both of which require large force generation from swimming and digging, on the other end. Furthermore, the locomotor-specific landscapes revealed that covariation of the appendicular and axial skeletons facilitate adaptations to each of these locomotor behaviors. These trade-offs are largely independent of size effects because body size variation scales from the top-left to bottom-right of morphospace whereas the trade-offs scale from the top-right to the bottom-left (Fig. 3; Fig. 4; Fig. S2). Sensitivity analyses examining the performance surfaces and adaptive landscapes using non-size corrected morphological traits confirm this pattern (see Supplementary Materials).

The majority of cursorial carnivorans occupy regions of morphospace that corresponded to the highest regions of the cursorial landscape. This landscape indicates that the appendicular and axial skeletons of cursorial carnivorans are functionally adapted for increased stride length through elongation of forelimb and increased sagittal flexibility of the full vertebral column (Fig. 3C; Table S2). As described above, these adaptations increase running speeds and reduce the energetic cost of transport by prioritizing dorsoventral flexion and extension in the sagittal plane [60–65,74–77,80].

At the other extreme, the appendicular and axial skeletons of semi-aquatic and semi-fossorial carnivorans are functionally adapted for increased elbow and knee extension through enlarged elements of the limbs and increased axial rotation in the vertebral column (Fig. 3E, F; Table S2). It is well documented that adaptations in the elbows and knees facilitate the ability to generate large power strokes for turning and stabilizing the body while swimming [39,58,72,73]. These similar adaptations also enable semi-fossorial species to generate large forces to dig [39,59,67,69–71] and improve stability and load transfer during clearing [59,67,73,86]. What

remains largely undetermined is the importance of increased axial joint rotation during swimming or digging. Presumably, for swimmers, torsional rotation of the intervertebral joints increases the maneuverability and ability to perform rapid turns in water [87,88]. Fully aquatic seals exhibit more flexible and compliant intervertebral joints compared to terrestrial mammals [85]; whether their joints are also more capable for torsional rotation remains to be studied. For semi-fossorial carnivorans, increased axial rotation of the vertebral column may provide additional leverage when digging through sediment. Evidence for increased axial rotation has been observed in the semi-fossorial nine-banded armadillo; experimentation on intervertebral joint flexion in this species revealed rotational motion in the joints despite not being explicitly tested [89]. Nonetheless, the benefits of increased joint rotation for digging remains puzzling. Interestingly, no carnivorans, including semi-aquatic and semi-fossorial species, occupied the highest regions of semi-aquatic or semi-fossorial landscapes. A likely explanation was that further axial rotation is biologically impossible for these carnivorans given their vertebral morphology that may be under evolutionary constraints having originated from terrestrial carnivorans. Thus, semi-aquatic and semi-fossorial carnivorans may already be at the highest region of the adaptive landscape that is biologically feasible.

The remaining locomotor landscapes were heavily weighted for sagittal mobility of the pre-diaphragmatic thoracic region (Fig. 3; Table S2). That the arboreal landscape was not heavily weighted by additional functional proxies is surprising considering that arboreality is often described as a specialized form of locomotion [90]. A possible explanation was that carnivorans do not display the full diversity of arboreal behaviors (e.g., brachiation, leaping, suspensory climbing) performed by other mammals. Another possibility was that we did not include all possible functional proxies in our analyses. For example, the ratio between proximal

manual phalanx length and metacarpal length has been shown to accurately predict climbing frequency in rodents [91], and thus may have altered the optimized weights of the arboreal adaptive landscape if this proxy or others were included in this current study. These unaccounted sources may also explain why arboreal species lie away from the highest regions of the adaptive landscape (Fig. 3B).

Adaptive landscapes optimized based on family also demonstrated similar patterns as locomotor-specific landscapes (Fig. 4). Most family-specific landscapes were heavily weighted for sagittal mobility of the pre-diaphragmatic thoracic region. Canids, which primarily exhibit cursorial or terrestrial hunting behaviors, exhibited similar patterns with the cursorial landscape with increased sagittal mobility in other regions of the vertebral column and elongation of the forelimb (Fig. 4G). Likewise, mephitids and mustelids comprise of many semi-aquatic and semi-fossorial species and thus exhibited similar patterns with the semi-aquatic and semi-fossorial landscapes of increased intervertebral joint rotation and enlarged limb joints (Fig. 4I, K). Adaptive landscapes for hyaenids and ursids were both unique compared to other family-specific landscapes (Table S6). The hyaenid landscape was heavily weighted for relative elongation of the forelimb (Fig. 4D); however, a caveat was that our low sample size of just two species reflected a biased representation of taxa with elongate forelimb and sloped back found in their extant diversity. Lastly, the ursid landscape was heavily weighted for increased intervertebral joint stiffness of the thoracolumbar vertebrae and increased robustness of the stylopodia of the limbs (Fig. 4H). These results were unsurprising as ursids are the biggest terrestrial carnivorans and these traits support their heavy bodies against the effects of gravity [13,66].

Lastly, we found that adaptive landscapes optimized based on dietary ecology were distinguished from each other based on the presence of terrestrial vertebrate prey in their diets,

which in turn can be partially explained by locomotor mode. In carnivorous and omnivorous carnivorans, a variety of hunting behaviors such as pursuing, ambush, pouncing, and digging behaviors were used to capture prey. Therefore, optimizing the landscape based on just carnivory masked these locomotor specializations and thus our ability to detect trade-offs and covariation among functional proxies. As a result, the carnivore and omnivore landscapes could not be distinguished from the combined landscape and were all heavily weighted for sagittal mobility of the pre-diaphragmatic thoracic region (Fig. S2; Table S4). In contrast, the herbivore, insectivore, and piscivore landscapes were all heavily weighted for increased joint torsion in the cervical and lumbar regions and larger femoral epicondyles (Fig. S2; Table S4), functional proxies that were also heavily weighted for semi-aquatic and semi-fossorial carnivorans. These results suggested that adaptations for swimming and digging behaviors not only dictate the functional landscape but may also help facilitate insectivorous and piscivorous diets; that is, they need to swim or dig for their prey. Nevertheless, our functional proxies for feeding consisted of just the mechanical advantage of jaw closure and thus may not capture the full functional diversity found in carnivorans. Inclusion of additional functional proxies from the cranium, mandible, and dentition may uncover further important contributions of the skull in the evolution of carnivorans [32–34,92].

Although biomechanical and ecomorphological studies have linked many of our selected functional proxies with performance traits [13,39,51–54], we acknowledge that our analyses were based on morphological proxies of function rather than empirical performance traits. These may affect the findings presented in this study. Future work incorporating empirical functional traits in adaptive landscape analyses requires the continual collection of performance, behavioral, and natural history data across the entire clade.

The carnivorans adaptive landscape is relatively flat

Many carnivoran skeletal components (e.g., mandible, dentition, hindlimb, and post-diaphragmatic region of the vertebral column) exhibit a short phylogenetic half-life relative to the age of Carnivora, suggesting that skeletal traits are strongly pulled towards distinct ecological peaks or clade-based adaptive zones across the adaptive landscape [23,33,34,48]. Surprisingly, we found that the topology of the carnivoran performance surfaces and optimized adaptive landscapes were largely characterized as smooth, gradual gradients between regions of low and high adaptive zones rather than as rugged, multipeak landscapes. Many-to-one mapping [93] may explain this decoupling between form and function. Multiple combinations of morphological traits may lead to the same functional outcome, resulting in a flat landscape that does not capture the rugged morphological landscape that was previously hypothesized.

The presence of a relatively flat topology may also indicate that carnivorans already occupy a broad adaptive zone relative to the overall mammalian adaptive landscape. Although carnivorans exhibit diverse locomotor modes and correspondingly diverse morphological adaptations, this diversity does not match the extreme locomotor and morphological specialization found in other mammalian clades, especially in the appendicular skeleton such as cranially facing forelimbs in subterranean moles [94], digit reduction in cursorial perissodactyls [95], and bipedalism in many saltatorial mammals [96]. Many of these specialized mammals may be constrained by their highly derived morphology and thus are adapted to optimize performance for just a single specialized locomotor behavior. That is, most locomotor modes cannot be maximized simultaneously and must trade off with other locomotor modes. In contrast, most carnivorans can perform multiple locomotor behaviors well including running, climbing,

digging, and swimming. For example, even the most cursorial carnivoran, the cheetah, can climb trees whereas no cursorial ungulate can. Therefore, the relatively flat landscape in carnivorans signals that functional trade-offs among locomotor performances cannot lead to highly derived specializations, which, in turn, may lead to rugged, multi-peak landscapes in other mammals. Instead, this carnivoran topology highlights that the even slight functional trade-offs across smooth, gradual gradients among appendicular and axial functional proxies can facilitate diverse locomotor modes as well as be flexible enough to enable additional locomotor behaviors. Future work "zooming out" of the carnivoran landscape will further elucidate how the relationships among functional trade-offs, relative degrees of morphological and ecological specializations, and landscape topologies differ among the various clades across Mammalia.

Acknowledgements

On title page

Funding

On title page

Authors' contributions

On title page

Figures

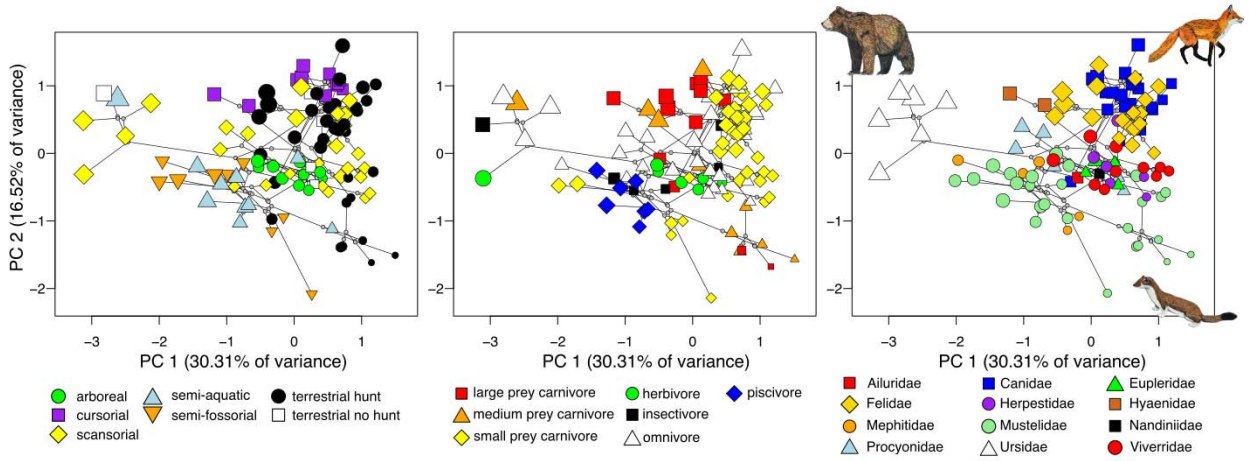

Fig. 1. Phylomorphospace of the carnivoran skeletal system defined by principal components (PCs) 1 and 2. PCA was conducted using 136 linear and angular measurements that capture morphological variation across the skull, appendicular, and axial skeletons (Table S1 shows trait loadings). Linear measurements were size-corrected using log shape ratios. Size of points are scaled to estimated body size based on the geometric mean of all measurements.

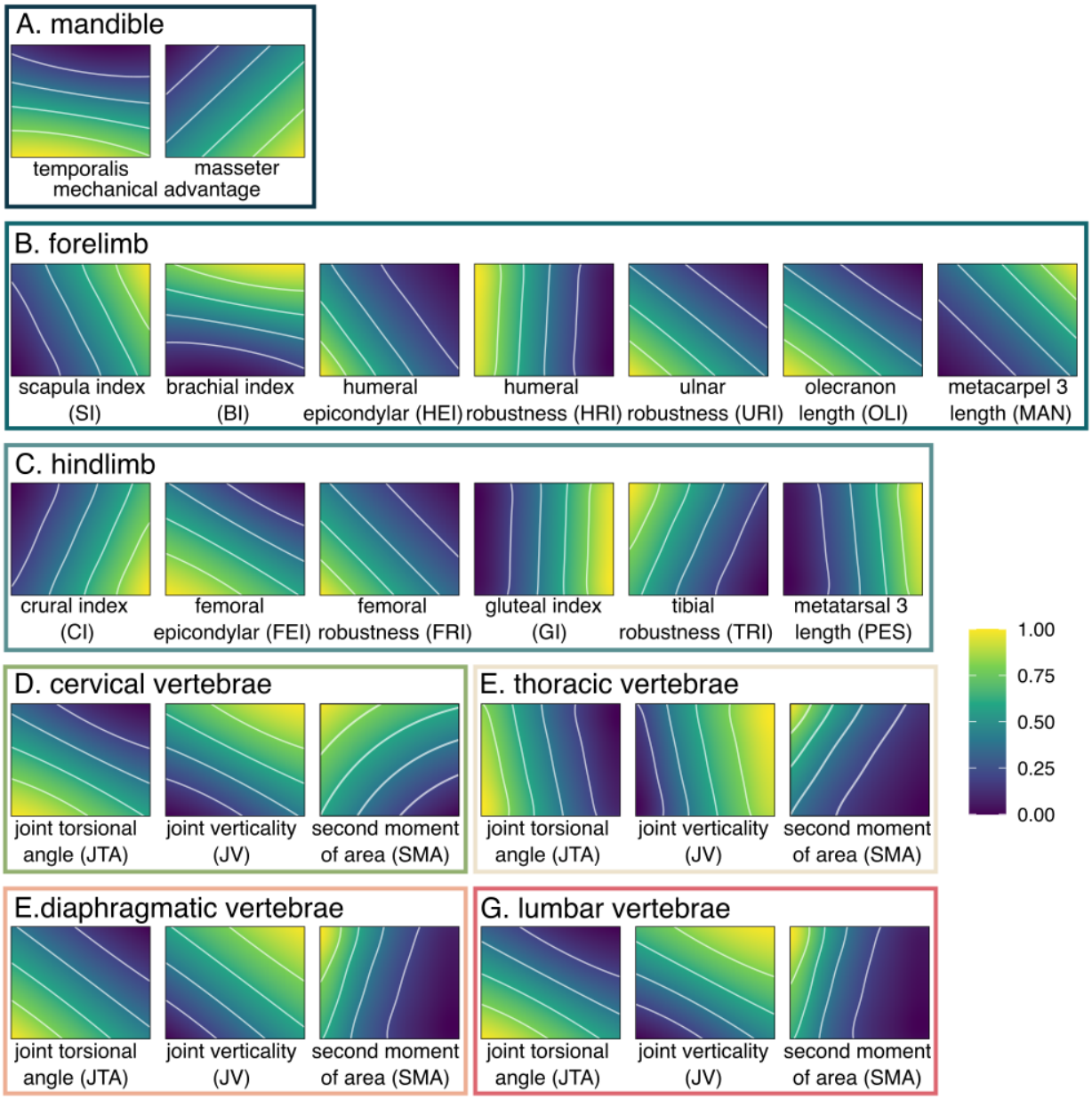

Fig. 2. Performance surfaces for each functional proxy. Color represents height on the performance surface. See Table 1 for functional proxies definitions.

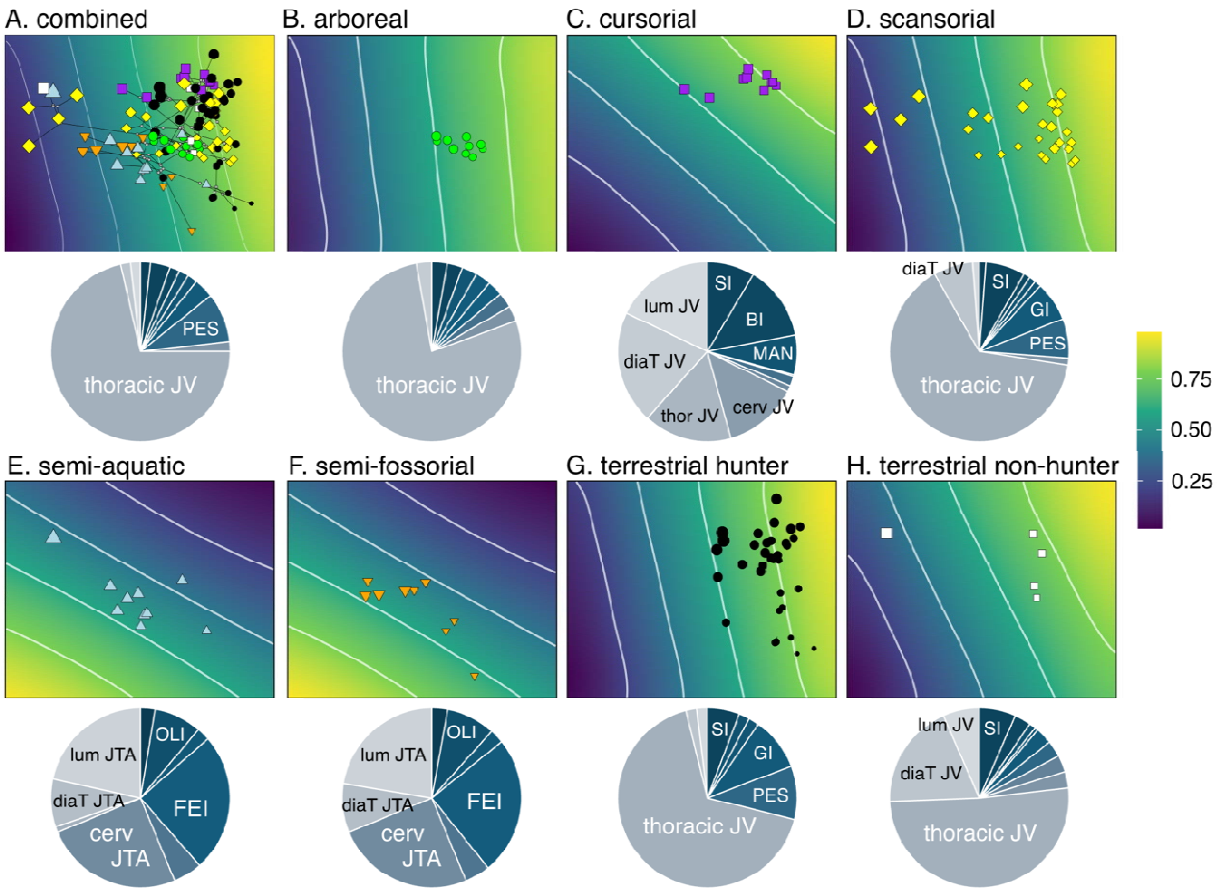

Fig. 3. Adaptive landscapes optimized for all carnivorans and each locomotor group. Landscapes were produced by combining the performance surfaces and optimizing their weightings to maximize the height of the landscape at the group mean. Pie charts show the relative weights of each performance surface on each landscape (Table S2 shows breakdown of weights). Functional proxies with weights > 0.07 were labeled. Table 2 shows statistical tests comparing adaptive landscapes among locomotor groups. Size of points are scaled to estimated body size based on the geometric mean of all measurements.

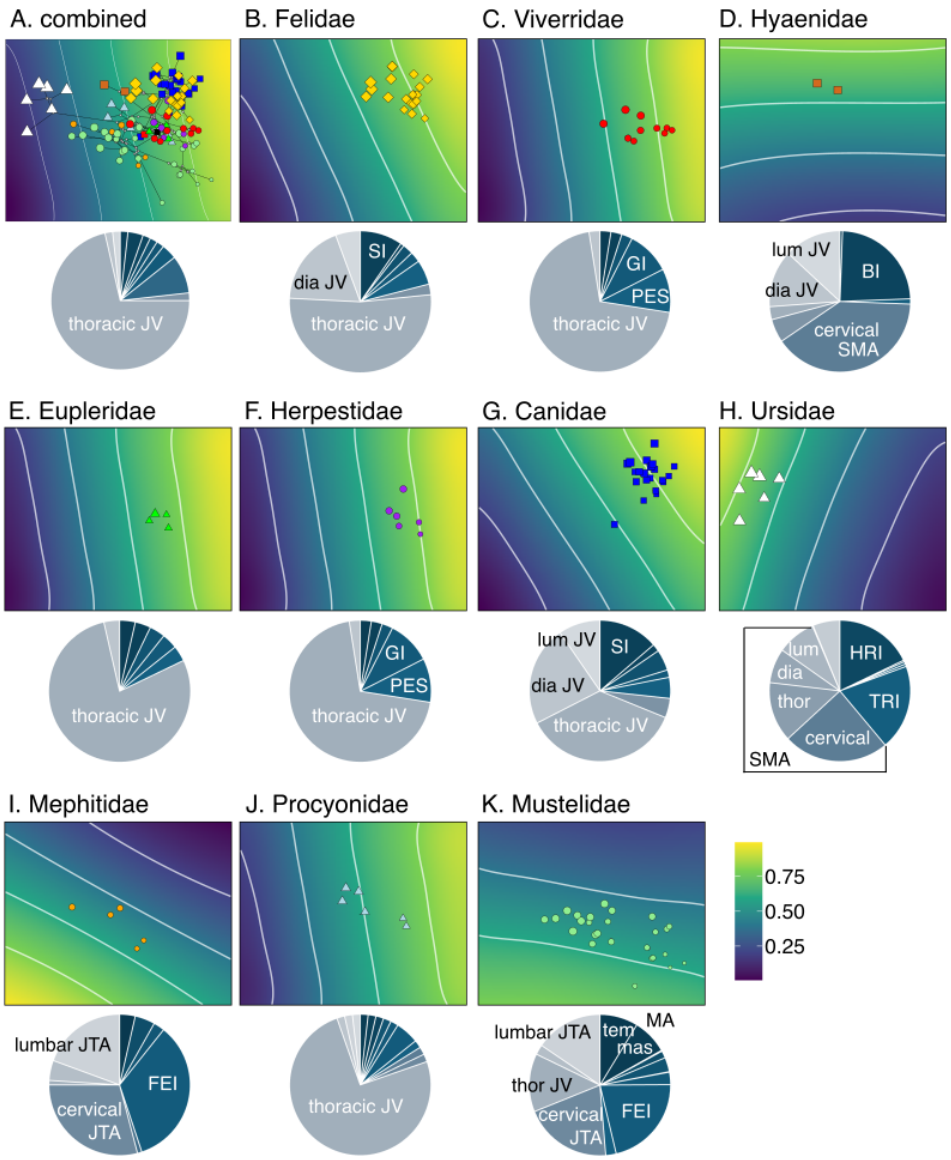

Fig. 4. Adaptive landscapes optimized for all carnivorans and each family. Landscapes were produced by combining the performance surfaces and optimizing their weightings to maximize the height of the landscape at the group mean. Pie charts show the relative weights of each performance surface on each adaptive landscape (Table S5 shows breakdown of weights). Functional proxies with weights > 0.09 were labeled. Table S6 shows statistical tests comparing adaptive landscapes among families. Size of points are scaled to estimated body size based on the geometric mean of all measurements.

Tables

Table 1. Functional proxies capturing the functional diversity of the skull [51], limbs [39,52], and vertebral column [13,53,54]. The full performance, biomechanical, and/or ecomorphological justification for each functional proxy is expanded upon in the Supplementary Materials.

Functional proxy	Description
Skull	
temporalis mechanical advantage (temMA)	Estimates how much force is produced at the bite point from force being input by the temporalis muscle
masseter mechanical advantage (masMA)	Estimates how much force is produced at the bite point from force being input by the masseter muscle
Forelimb	
Scapula index (SI)	Describes the expansion of shoulder musculature versus contribution of scapula to limb elongation.
Brachial index (BI)	Estimates the relative proportions of the proximal and distal elements of the forelimb and serves as an index of the relative distal out-lever length.
Humeral robustness index (HRI)	Estimates the robustness of the humerus and its ability to resist bending and shearing stresses.
Humeral epicondylar index (HEI)	Estimates the relative area of the distal end of the humerus available for the origins of the forearm flexors, pronators, and supinators.
Olecranon length index (OLI)	Estimates the relative mechanical advantage of the triceps brachii and dorsoepitrochlearis muscles used in elbow extension.
Ulnar robustness index (URI)	Estimates the robustness of the ulna and its ability to resist bending and shearing stresses, and relative area available for the origin and insertion of forearm and manus flexors, pronators, and supinators.
Manus proportions index (MAN)	Estimates the relative proportions of proximal and distal elements of the forelimb, and relative size of the hand.
Hindlimb	
Crural index (CI)	Estimates relative proportions of proximal and distal elements of the hind limb.
Femoral robustness index (FRI)	Estimates robustness of the femur and its ability to resist bending and shearing stresses.

Gluteal index (GI)	Estimates the relative mechanical advantage of the gluteal muscles used in retraction of the femur.
Femoral epicondylar index (FEI)	Estimates relative area available for the origins of the gastrocnemius and soleus muscles used in extension of the knee and plantar-flexion of the pes.
Tibial robustness index (TRI)	Estimates robustness of the tibia and its ability to resist bending and shearing stresses.
Pes length index (PES)	Estimates relative proportions of proximal and distal elements of the hind limb, and relative size of the hind foot.
Vertebrae	
Sagittal second moment of area (sSMA)	Estimates stiffness in the of the vertebral joint in the sagittal plane.
Lateral second moment of area (lSMA)	Estimates stiffness in the of the vertebral joint in the lateral plane.
Joint torsional angle (JTA)	Estimates the degree of axial torsion of the vertebrae.
Joint verticality (JV)	Estimates the relative importance of sagittal bending versus lateral bending of vertebral joints.

Table 2. Pairwise significance tests among locomotor adaptive landscapes. Top triangle: number of landscape models shared in the top 5% between the paired groups. Bottom triangle: P-values for difference between groups. Bolded P-values indicate significance.

	arboreal	cursorial	scansorial	semi-aquatic	semi-fossorial	terrestrial hunter	terrestrial non-hunter
arboreal	-	4	7	0	0	6	6
cursorial	0.400	-	10	0	0	7	34
scansorial	0.700	**0.033**	-	0	0	14	15
semi-aquatic	**0.001**	**0.001**	**0.001**	-	88	0	0
semi-fossorial	**0.001**	**0.001**	**0.001**	0.917	-	0	0
terrestrial hunter	0.600	**0.023**	0.778	**0.001**	**0.001**	-	12
terrestrial nonhunter	0.600	0.114	0.833	**0.001**	**0.001**	0.857	-

References

1. Arnold SJ. 1983 Morphology, performance and fitness. *Amer. Zool.* **23**, 347–361. (doi:10.1554/05-647.1)

2. Wainwright PC. 1994 Functional morphology as a tool in ecological research. In *Ecological Morphology Integrative Organismal Biology* (eds PC Wainwright, SM Reilly), Ecological Morphology: Integrative ….

3. Higham TE *et al.* 2021 Linking ecomechanical models and functional traits to understand phenotypic diversity. *Trends in Ecology & Evolution* , 1–14. (doi:10.1016/j.tree.2021.05.009)

4. Law CJ, Duran E, Hung N, Richards E, Santillan I, Mehta RS. 2018 Effects of diet on cranial morphology and biting ability in musteloid mammals. *J. Evol. Biol.* **31**, 1918–1931. (doi:10.1111/jeb.13385)

5. Santana SE, Dumont ER, Dumont E, Davis JL. 2010 Mechanics of bite force production and its relationship to diet in bats. *Funct. Ecol.* **24**, 776–784. (doi:10.1111/j.1365-2435.2010.01703.x)

6. Tseng ZJ, Garcia-Lara S, Flynn JJ, Holmes E, Rowe TB, Dickson BV. 2023 A switch in jaw form–function coupling during the evolution of mammals. *Philos. Trans. R. Soc. B* **378**, 20220091. (doi:10.1098/rstb.2022.0091)

7. Collar DC, Reece JS, Alfaro ME, Wainwright PC. 2014 Imperfect morphological convergence: variable changes in cranial structures underlie transitions to durophagy in moray eels. *Am Nat* **183**, E168–E184. (doi:10.5061/dryad.h9r37)

8. Sustaita D, Pouydebat E, Manzano A, Abdala V, Hertel F, Herrel A. 2013 Getting a grip on tetrapod grasping: form, function, and evolution. *Biol. Rev.* **88**, 380–405. (doi:10.1111/brv.12010)

9. Amson E, Bibi F. 2021 Differing effects of size and lifestyle on bone structure in mammals. *BMC Biol.* **19**, 87. (doi:10.1186/s12915-021-01016-1)

10. Sansalone G, Castiglione S, Raia P, Archer M, Dickson B, Hand S, Piras P, Profico A, Wroe S. 2020 Decoupling Functional and Morphological Convergence, the Study Case of Fossorial Mammalia. *Frontiers Earth Sci* **8**, 112. (doi:10.3389/feart.2020.00112)

11. Dickson BV, Pierce SE. 2019 Functional performance of turtle humerus shape across an ecological adaptive landscape. *Evolution* **73**, 1265–1277. (doi:10.1111/evo.13747)

12. Law CJ, Slater GJ, Mehta RS. 2019 Shared extremes by ectotherms and endotherms: Body elongation in mustelids is associated with small size and reduced limbs. *Evolution* **73**, 735–749. (doi:10.1111/evo.13702)

13. Jones KE, Dickson BV, Angielczyk KD, Pierce SE. 2021 Adaptive landscapes challenge the "lateral-to-sagittal" paradigm for mammalian vertebral evolution. *Curr. Biol.* **31**, 1883-1892.e7. (doi:10.1016/j.cub.2021.02.009)

14. Jones KE, Benitez L, Angielczyk KD, Pierce SE. 2018 Adaptation and constraint in the evolution of the mammalian backbone. *Bmc Evol Biol* **18**, 172. (doi:10.1186/s12862-018-1282-2)

15. Polly PD, Stayton CT, Dumont ER, Pierce SE, Rayfield EJ, Angielczyk KD. 2016 Combining Geometric Morphometrics and Finite Element Analysis with Evolutionary Modeling: Towards a Synthesis. *J Vertebr Paleontol* **36**, e1111225. (doi:10.1080/02724634.2016.1111225)

16. Stayton CT. 2019 Performance in three shell functions predicts the phenotypic distribution of hard□shelled turtles. *Evolution* **73**, 720–734. (doi:10.1111/evo.13709)

17. Arnold SJ, Pfrender ME, Jones AG. 2001 The adaptive landscape as a conceptual bridge between micro- and macroevolution. *Genetica* **112–113**, 9–32. (doi:10.1023/a:1013373907708)

18. Hansen TF. 1997 Stabilizing selection and the comparative analysis of adaptation. *Evolution* **51**, 1341–1351. (doi:10.1111/j.1558-5646.1997.tb01457.x)

19. Butler MA, King AA. 2004 Phylogenetic comparative analysis: a modeling approach for adaptive evolution. *Am Nat* **164**, 683–695. (doi:10.1086/426002)

20. Beaulieu JM, Jhwueng D-C, Boettiger C, O'Meara BC. 2012 Modeling stabilizing selection: Expanding the Ornstein-Uhlenbeck model of adaptive evolution. *Evolution* **66**, 2369–2383. (doi:10.1111/j.1558-5646.2012.01619.x)

21. Uyeda JC, Harmon LJ. 2014 A novel Bayesian method for inferring and interpreting the dynamics of adaptive landscapes from phylogenetic comparative data. *Syst. Biol.* **63**, 902–918. (doi:10.1093/sysbio/syu057)

22. Bastide P, Ané C, Robin S, Mariadassou M. 2018 Inference of Adaptive Shifts for Multivariate Correlated Traits. *Syst. Biol.* **67**, 662–680. (doi:10.1093/sysbio/syy005)

23. Slater GJ. 2022 Topographically distinct adaptive landscapes for teeth, skeletons, and size explain the adaptive radiation of Carnivora (Mammalia). *Evolution* (doi:10.1111/evo.14577)

24. Law CJ. 2022 Different Evolutionary Pathways Lead to Incomplete Convergence of Elongate Body Shapes in Carnivoran Mammals. *Systematic Biol* **71**, 788–796. (doi:10.1093/sysbio/syab091)

25. Friedman ST, Price SA, Hoey AS, Wainwright PC. 2016 Ecomorphological convergence in planktivorous surgeonfishes. *J. Evol. Biol.* **29**, 965–978. (doi:10.1111/jeb.12837)

26. Arbour JH, Curtis AA, Santana SE. 2019 Signatures of echolocation and dietary ecology in the adaptive evolution of skull shape in bats. *Nat Commun* **10**, 2036. (doi:10.1038/s41467-019-09951-y)

27. Price SA, Hopkins SSB. 2015 The macroevolutionary relationship between diet and body mass across mammals. *Biol J Linn Soc* **115**, 173–184. (doi:10.1111/bij.12495)

28. Zelditch ML, Ye J, Mitchell JS, Swiderski DL. 2017 Rare ecomorphological convergence on a complex adaptive landscape: Body size and diet mediate evolution of jaw shape in squirrels (Sciuridae). *Evolution* **71**, 633–649. (doi:10.1111/evo.13168)

29. Dickson BV, Clack JA, Smithson TR, Pierce SE. 2021 Functional adaptive landscapes predict terrestrial capacity at the origin of limbs. *Nature* **589**, 242–245. (doi:10.1038/s41586-020-2974-5)

30. Radinsky LB. 1981 Evolution of skull shape in Carnivores .1. Representative modern Carnivores. *Biol J Linn Soc* **15**, 369–388. (doi:10.1111/j.1095-8312.1981.tb00770.x)

31. Valkenburgh BV. 2007 Deja vu: the evolution of feeding morphologies in the Carnivora. *Amer. Zool.* **47**, 147–163. (doi:10.1093/icb/icm016)

32. Tseng ZJ, Flynn JJ. 2018 Structure-function covariation with nonfeeding ecological variables influences evolution of feeding specialization in Carnivora. *Sci Adv* **4**, eaao5441. (doi:10.1126/sciadv.aao5441)

33. Slater GJ, Friscia AR. 2019 Hierarchy in adaptive radiation: A case study using the Carnivora (Mammalia). *Evolution* **73**, 524–539. (doi:10.1111/evo.13689)

34. Law CJ, Blackwell EA, Curtis AA, Dickinson E, Hartstone□Rose A, Santana SE. 2022 Decoupled evolution of the cranium and mandible in carnivoran mammals. *Evolution* **76**, 2959–2974. (doi:10.1111/evo.14578)

35. Figueirido B, MacLeod N, Krieger J, Renzi MD, Pérez-Claros JA, Palmqvist P. 2011 Constraint and adaptation in the evolution of carnivoran skull shape. *Paleobiology* **37**, 490–518. (doi:10.1666/09062.1)

36. Valkenburgh BV. 1985 Locomotor diversity within past and present guilds of large predatory mammals. *Paleobiology* **11**, 406–428. (doi:10.1017/s0094837300011702)

37. Valkenburgh BV. 1987 Skeletal indicators of locomotor behavior in living and extinct carnivores. *J Vertebr Paleontol* **7**, 162–182. (doi:10.1080/02724634.1987.10011651)

38. Iwaniuk AN, Pellis SM, Whishaw IQ. 1999 The relationship between forelimb morphology and behaviour in North American carnivores (Carnivora). *Can J Zool* **77**, 1064–1074. (doi:10.1139/z99-082)

39. Samuels JX, Meachen JA, Sakai SA. 2013 Postcranial morphology and the locomotor habits of living and extinct carnivorans. *J Morpho* **274**, 121–146. (doi:10.1002/jmor.20077)

40. Martín-Serra A, Figueirido B, Palmqvist P. 2014 A three-dimensional analysis of the morphological evolution and locomotor behaviour of the carnivoran hind limb. *BMC Evol Biol* **14**, 1–13. (doi:10.1186/1471-2148-14-129)

41. Martín-Serra A, Figueirido B, Palmqvist P. 2014 A Three-Dimensional Analysis of Morphological Evolution and Locomotor Performance of the Carnivoran Forelimb. *Plos One* **9**, e85574. (doi:10.1371/journal.pone.0085574)

42. Randau M, Cuff AR, Hutchinson JR, Pierce SE, Goswami A. 2017 Regional differentiation of felid vertebral column evolution: a study of 3D shape trajectories. *Org Divers Evol* **17**, 1–15. (doi:10.1007/s13127-016-0304-4)

43. Figueirido B, Martín-Serra A, Pérez-Ramos A, Velasco D, Pastor FJ, Benson RJ. 2021 Serial disparity in the carnivoran backbone unveils a complex adaptive role in metameric evolution. *Communications Biology* , 1–15. (doi:10.1038/s42003-021-02346-0)

44. Martín-Serra A, Pérez-Ramos A, Pastor FJ, Velasco D, Figueirido B. 2021 Phenotypic integration in the carnivoran backbone and the evolution of functional differentiation in metameric structures. *Evolution Letters* , 1–14. (doi:10.1002/evl3.224)

45. Law CJ. 2021 Ecological drivers of carnivoran body shape evolution. *Am Nat* **198**, 406–420. (doi:10.5061/dryad.pg4f4qrpm)

46. Law CJ. 2021 Evolutionary and morphological patterns underlying carnivoran body shape diversity. *Evolution* **75**, 365–375. (doi:10.1111/evo.14143)

47. Uyeda JC, Zenil-Ferguson R, Pennell MW. 2018 Rethinking phylogenetic comparative methods. *Syst. Biol.* **67**, 1091–1109. (doi:10.1093/sysbio/syy031)

48. Law CJ, Hlusko LJ, Tseng ZJ. 2024 Uncovering the mosaic evolution of the carnivoran skeletal system. *Biol. Lett.* **20**, 20230526. (doi:10.1098/rsbl.2023.0526)

49. Humphreys AM, Barraclough TG. 2014 The evolutionary reality of higher taxa in mammals. *Proc Royal Soc B Biological Sci* **281**, 20132750. (doi:10.1098/rspb.2013.2750)

50. Law CJ. 2019 Solitary meat-eaters: solitary, carnivorous carnivorans exhibit the highest degree of sexual size dimorphism. *Sci Rep-uk* **9**, 15344. (doi:10.1038/s41598-019-51943-x)

51. Greaves WS. 2012 The Mammalian Jaw. , 3–25. (doi:10.1017/cbo9781139060851.003)

52. Davis DD. 1964 *The giant panda: a morphological study of evolutionary mechanisms*. Fieldiana (Zoology Memoirs). (doi:10.5962/bhl.title.5133)

53. Jones KE, Gonzalez S, Angielczyk KD, Pierce SE. 2020 Regionalization of the axial skeleton predates functional adaptation in the forerunners of mammals. *Nat Ecol Evol* **4**, 470–478. (doi:10.1038/s41559-020-1094-9)

54. Boszczyk BM, Boszczyk AA, Putz R. 2001 Comparative and functional anatomy of the mammalian lumbar spine. *Anatomical Rec* **264**, 157–168. (doi:10.1002/ar.1156)

55. Muñoz NA. 2020 Locomotion in Rodents and Small Carnivorans: Are they So Different? *Journal of Mammalian Evolution* , 1–12. (doi:10.1007/s10914-020-09515-8)

56. Marshall SK, Spainhower KB, Sinn BT, Diggins TP, Butcher MT. 2021 Hind Limb Bone Proportions Reveal Unexpected Morphofunctional Diversification in Xenarthrans. *J. Mamm. Evol.* **28**, 599–619. (doi:10.1007/s10914-021-09537-w)

57. Hedrick BP, Dickson BV, Dumont ER, Pierce SE. 2020 The evolutionary diversity of locomotor innovation in rodents is not linked to proximal limb morphology. *Scientific Reports* , 1–11. (doi:10.1038/s41598-019-57144-w)

58. Kilbourne BM. 2017 Selective regimes and functional anatomy in the mustelid forelimb: Diversification toward specializations for climbing, digging, and swimming. *Ecol Evol* **66**, 2369–12. (doi:10.1002/ece3.3407)

59. Rickman J, Burtner AE, Linden TJ, Santana SE, Law CJ. 2023 Size And Locomotor Ecology Have Differing Effects on the External and Internal Morphologies of Squirrel (Rodentia: Sciuridae) Limb Bones. *Integr. Org. Biol.* **5**, obad017. (doi:10.1093/iob/obad017)

60. Strang KT, Steudel K. 1990 Explaining the scaling of transport costs: the role of stride frequency and stride length. *J. Zoo□l.* **221**, 343–358. (doi:10.1111/j.1469-7998.1990.tb04006.x)

61. Kram R, Taylor CR. 1990 Energetics of running: a new perspective. *Nature* **346**, 265–267. (doi:10.1038/346265a0)

62. Garland T, Janis CM. 1993 Does metatarsal/femur ratio predict maximal running speed in cursorial mammals? *J. Zoo□l.* **229**, 133–151. (doi:10.1111/j.1469-7998.1993.tb02626.x)

63. Kilbourne BM, Hoffman LC. 2013 Scale Effects between Body Size and Limb Design in Quadrupedal Mammals. *PLoS ONE* **8**, e78392. (doi:10.1371/journal.pone.0078392)

64. Pontzer H. 2007 Effective limb length and the scaling of locomotor cost in terrestrial animals. *J. Exp. Biol.* **210**, 1752–1761. (doi:10.1242/jeb.002246)

65. Pontzer H. 2007 Predicting the energy cost of terrestrial locomotion: a test of the LiMb model in humans and quadrupeds. *J. Exp. Biol.* **210**, 484–494. (doi:10.1242/jeb.02662)

66. Polly PD. 2007 Limbs in mammalian evolution. In *Fins into Limbs Evolution, Development, and Transformation* (ed BK Hall), pp. 245–268. Fins into Limbs Evolution, Development, and Transformation.

67. Hildebrand M. 1985 Digging of Quadrupeds. In *Functional Vertebrate Morphology* (eds M Hildebrand, DM Bramble, KF Liem, DB Wake), pp. 89–109. Cambridge, MA: Harvard University Press. (doi:10.4159/harvard.9780674184404.c6)

68. Nakai D, Fujiwara S. 2023 Fossorial mammals emphasise the forelimb muscle moment arms used for digging: New indices for reconstruction of the digging ability and behaviours in extinct taxa. *J. Anat.* **242**, 846–861. (doi:10.1111/joa.13815)

69. Lessa EP, Stein BR. 1992 Morphological constraints in the digging apparatus of pocket gophers (Mammalia: Geomyidae). *Biol J Linn Soc* **47**, 439–453. (doi:10.1111/j.1095-8312.1992.tb00678.x)

70. Lagaria A, Youlatos D. 2006 ANATOMICAL CORRELATES TO SCRATCH DIGGING IN THE FORELIMB OF EUROPEAN GROUND SQUIRRELS (SPERMOPHILUS CITELLUS). *J Mammal* **87**, 563–570. (doi:10.1644/05-mamm-a-251r1.1)

71. Rose J, Moore A, Russell A, Butcher M. 2014 Functional osteology of the forelimb digging apparatus of badgers. *J. Mammal.* **95**, 543–558. (doi:10.1644/13-mamm-a-174)

72. Fish FE. 2000 Biomechanics and Energetics in Aquatic and Semiaquatic Mammals: Platypus to Whale*. *Physiol Biochem Zool* **73**, 683–698. (doi:10.1086/318108)

73. Samuels JX, Valkenburgh BV. 2008 Skeletal indicators of locomotor adaptations in living and extinct rodents. *J Morpho* **269**, 1387–1411. (doi:10.1002/jmor.10662)

74. Gambaryan PP. 1974 *How Mammals Run: Anatomical Adaptations*. J. Wiley.

75. Schilling N, Hackert R. 2006 Sagittal spine movements of small therian mammals during asymmetrical gaits. *J. Exp. Biol.* **209**, 3925–3939. (doi:10.1242/jeb.02400)

76. Hildebrand M. 1959 Motions of the Running Cheetah and Horse. *J. Mammal.* **40**, 481–495. (doi:10.2307/1376265)

77. Hildebrand M. 1985 Walking and Running. In *Functional Vertebrate Morphology* (eds M Hildebrand, DM Bramble, KF Liem, DB Wake), pp. 38–57. Cambridge, MA: Harvard University Press. (doi:10.4159/harvard.9780674184404.c3)

78. Belyaev RI, Kuznetsov AN, Prilepskaya NE. 2022 From dorsomobility to dorsostability: A study of lumbosacral joint range of motion in artiodactyls. *J. Anat.* **241**, 420–436. (doi:10.1111/joa.13688)

79. Belyaev RI, Kuznetsov AN, Prilepskaya NE. 2021 How the even□toed ungulate vertebral column works: Comparison of intervertebral mobility in 33 genera. *J. Anat.* **239**, 1370–1399. (doi:10.1111/joa.13521)

80. Belyaev RI, Nikolskaia P, Bushuev AV, Panyutina AA, Kozhanova DA, Prilepskaya NE. 2023 Running, jumping, hunting, and scavenging: Functional analysis of vertebral mobility and backbone properties in carnivorans. *J. Anat.* (doi:10.1111/joa.13955)

81. Alexander RMcN, Dimery NJ, Ker RF. 1985 Elastic structures in the back and their rôle in galloping in some mammals. *J. Zoo□l.* **207**, 467–482. (doi:10.1111/j.1469-7998.1985.tb04944.x)

82. McMahon TA. 1985 The role of compliance in mammalian running gaits. *J. Exp. Biol.* **115**, 263–282. (doi:10.1242/jeb.115.1.263)

83. Taylor CR. 1978 Why Change Gaits? Recruitment of Muscles and Muscle Fibers as a Function of Speed and Gait. *Am. Zoo□l.* **18**, 153–161. (doi:10.1093/icb/18.1.153)

84. Koob TJ, Long JH. 2000 The Vertebrate Body Axis: Evolution and Mechanical Function1. *Am. Zoo□l.* **40**, 1–18. (doi:10.1668/0003-1569(2000)040[0001:tvbaea]2.0.co;2)

85. Gál JM. 1993 Mammalian Spinal Biomechanics: I. Static and Dynamic Mechanical Properties of Intact Intervertebral Joints. *J. Exp. Biol.* **174**, 247–280. (doi:10.1242/jeb.174.1.247)

86. Casinos A, Quintana C, Viladiu C. 1993 Allometry and adaptation in the long bones of a digging group of rodents (Ctenomyinae). *Zoo□l. J. Linn. Soc.* **107**, 107–115. (doi:10.1006/zjls.1993.1007)

87. Fish FE. 1994 Association of propulsive swimming mode with behavior in river otters (Lutra canadensis). *J Mammal* **75**, 989–997.

88. Fish FE, Hurley J, Costa DP. 2003 Maneuverability by the sea lion Zalophus californianus: turning performance of an unstable body design. *J. Exp. Biol.* **206**, 667–674. (doi:10.1242/jeb.00144)

89. Oliver JD, Jones KE, Hautier L, Loughry WJ, Pierce SE. 2016 Vertebral bending mechanics and xenarthrous morphology in the nine-banded armadillo (Dasypus novemcinctus). *J. Exp. Biol.* **219**, 2991–3002. (doi:10.1242/jeb.142331)

90. Young JW. 2023 Convergence of arboreal locomotor specialization: morphological and behavioral solutions for movement on narrow and compliant supports. In *Convergent evolution: Animal form and function*, pp. 289–322. Springer International Publishing. (doi:10.1007/978-3-031-11441-0_11)

91. Nations JA, Heaney LR, Demos TC, Achmadi AS, Rowe KC, Esselstyn JA. 2019 A simple skeletal measurement effectively predicts climbing behaviour in a diverse clade of small mammals. *Biol. J. Linn. Soc.* **128**, 323–336. (doi:10.1093/biolinnean/blz085)

92. Sansalone G, Wroe S, Coates G, Attard MRG, Fruciano C. 2024 Unexpectedly uneven distribution of functional trade-offs explains cranial morphological diversity in carnivores. *Nat. Commun.* **15**, 3275. (doi:10.1038/s41467-024-47620-x)

93. Wainwright PC, Alfaro ME, Bolnick DI, Hulsey CD. 2005 Many-to-one mapping of form to function: a general principle in organismal design? *Integr Comp Biol* **45**, 256–262. (doi:10.1093/icb/45.2.256)

94. Lin Y-F, Konow N, Dumont ER. 2019 How moles destroy your lawn: the forelimb kinematics of eastern moles in loose and compact substrates. *J. Exp. Biol.* **222**, jeb182436. (doi:10.1242/jeb.182436)

95. Economou G, McGrath M, Wajsberg J, Granatosky MC. 2021 Perissodactyla Locomotion. In *Encyclopedia of Animal Cognition and Behavior* (eds J Vonk, TK Shackelford), pp. 1–8. Switzerland: Springer Nature. (doi:10.1007/978-3-319-47829-6_887-1)

96. McGowan CP, Collins CE. 2018 Why do mammals hop? Understanding the ecology, biomechanics and evolution of bipedal hopping. *J. Exp. Biol.* **221**, jeb161661. (doi:10.1242/jeb.161661)

Supplementary Materials for

The carnivoran adaptive landscape reveals functional trade-offs among the skull, appendicular, and axial skeleton

Contains:

Supplementary Methods

Sensitivity Analyses

Fig. S1. Skeletal trait measurements used in this study.

Fig. S2. Adaptive landscapes optimized for each dietary group.

Fig. S3. Performance surfaces from Sensitivity Analyses 1.

Fig. S4. Adaptive landscape results from Sensitivity Analyses 2.

Fig. S5. Performance surfaces from Sensitivity Analyses 3.

Fig. S6. Adaptive landscapes results from Sensitivity Analyses 3.

Fig. S7. Phylomorphospace of the carnivoran skeletal system based on non-size corrected traits.

Fig. S8. Performance surfaces from Sensitivity Analyses 4.

Fig. S9. Adaptive landscapes from Sensitivity Analyses 4.

Table S1. PC loadings of skeletal traits.

Table S2. Relative weights of functional proxies optimized in the locomotor landscapes.

Table S3. Pairwise significance tests among dietary adaptive landscapes.

Table S4. Relative weights of functional proxies optimized in the dietary adaptive landscapes.

Table S5. Relative weights of functional proxies optimized in the familial adaptive landscapes.

Table S6. Pairwise significance tests among familial adaptive landscapes.

Table S7. Scaling matrix for the first linear discriminant function.

Table S8. Relative weights of landscapes from Sensitivity Analyses 2.

Table S9. Relative weights of locomotor adaptive landscapes from Sensitivity Analyses 4.

Table S10. Relative weights of dietary adaptive landscapes from Sensitivity Analyses 4.

Table S11. Relative weights of familial adaptive landscapes from Sensitivity Analyses 4.

References

Supplementary Methods

Creating the morphospace

We created a morphospace of 109 terrestrial carnivoran species (198 specimens) based on 136 linear and angular measurements that capture morphological variation across the entire skeleton (Fig. S1). This dataset includes seven cranial traits, seven mandibular traits, 13 forelimb traits, 13 hindlimb traits, and 11 traits each in the third cervical, fifth cervical, first thoracic, middle thoracic, diaphragmatic thoracic, last thoracic, first lumbar, middle lumbar and last lumbar vertebrae. We were able to incorporate representatives from 12 of the 13 extant terrestrial carnivoran families; specimens from Prionodontidae were unavailable. We removed size effects on linear measurements by calculating the log shape ratio (i.e., ln[trait/size]) of each skeletal trait, where size is the geometric mean of all linear trait measurements (see Sensitivity Analyses section for further investigation of the concern of using linear measurements with no size correction). We used only adult male specimens because carnivorans exhibit differing degrees of sexual dimorphism [1]. We then conducted a principal component analysis (PCA) using the covariance matrix on all size-corrected measurements and used the first two PC axes (46.7% of the total variance) to create the morphospace (Fig. 1; see Table S1 for PC loadings). Carnivoran species are widely distributed across the morphospace except for the bottom-left region in which

no species occupy (-PC1, -PC2). We chose not to run a phylogenetic PCA because we are interested in the primary dimensions of morphological variation regardless of phylogenetic structuring. In addition, pPCA is more difficult to interpret because it is a mixture of major axes that describe non-phylogenetic variation and scores that contain phylogenetic components of variation, and pPC axes are not orthogonal to each other, meaning that the first two axes (which we use for the adaptive landscape analyses) may include less variance explained than PCA by containing correlated variance components rather than independent ones [2].

Creating morphological proxies for function

To fully sample skeletal variation throughout the morphospace, we generated 63 theoretical species evenly across the morphospace in a 9 x 7 grid along the first two PCs. We then generated theoretical morphological traits from each of the 63 theoretical species by multiplying each eigenvector by each specified PC score and adding the mean of all 136 traits (see Sensitivity Analyses section for further investigation of the concerns of grid size and the use of theoretical species). From these theoretical morphological traits, we calculated 27 functional indices (Table 1) that capture the functional diversity of the skull [3], limbs [4,5], and vertebral column [6–8]:

<u>Functional proxies for the skull</u>

Temporalis mechanical advantage (temMA) = temporalis moment arm / distance from the jaw condyle to the carnassial. temMA estimates how much force is produced at the bite point from force being input by the temporalis muscle. Lever mechanics suggest that a high temMA indicates a jaw optimized for stronger bites whereas a low temMA indicates a jaw optimized for

faster bites. Biomechanical studies have found that increased temMA contributes to increased bite force [9–12].

Masseter mechanical advantage (masMA) = masseter moment arm / distance from the jaw condyle to the carnassial. masMA estimates how much force is produced at the bite point from force being input by the masseter muscle. Lever mechanics suggest that a high masMA indicates a jaw optimized for stronger bites whereas a low masMA indicates a jaw optimized for faster bites. Biomechanical studies have found that increased masMA contributes to increased bite force [9–12].

Functional proxies for the forelimb

Scapula index (SI) = scapula length / scapula height. SI describes the expansion of shoulder musculature versus contribution of scapula to limb elongation. The absence or reduction of the clavicle in several mammalian clades allows the scapula to move freely in the parasagittal plane and contribute to stride length [13–15]. Some view the scapula as the first element of the forelimb and thus serves as the functional equivalent to the femur in the hindlimb. Biomechanical analyses found that the proximal elements of the limb (i.e., scapula and femur) produce more than half of the propulsive movement of the whole limb at symmetrical gaits [16]. Although the relationship between these performance metrics and scapula shape remains to be tested, ecomorphological studies suggest that increased SI helps with increased stride length and thus tends to be associated with cursorial species, whereas decreased SI provides the teres major muscle with more efficient leverage for powerful adduction of the forelimb and thus tends to be associated with fossorial and natatorial species [14].

Brachial index (BI) = radius length / humerus length. BI estimates the relative proportions of the proximal and distal elements of the forelimb and serves as an index of the relative distal out-lever length. The relatively longer distal end of the forelimb facilitates increased stride length and decreased moment of inertia of limbs, which in turn decreases the energetic cost of transport [14,17–22]. Performance studies found that increased BI is correlated with faster running speeds [23]. Ecomorphological studies suggest that increased BI tends to be associated with cursorial species whereas decreased BI is associated with arboreal, natatorial, and fossorial species [4,5,24].

Humeral robustness index (HRI) = mediolateral diameter of humerus / humerus length. HRI estimates the robustness of the humerus and its ability to resist bending and shearing stresses. Performance studies found that increased HRI is correlated with lower stresses at yield, lower elastic moduli, and higher resistance to failure when a bending force is applied [25]. Ecomorphological studies suggest that increased HRI tends to be associated with fossorial and natatorial species whereas decreased HRI is associated with cursorial and scansorial species [5,24,26,27].

Humeral epicondylar index (HEI) = epicondylar breadth of humerus / humerus length. HEI estimates the relative area of the distal end of the humerus available for the origins of the forearm flexors, pronators, and supinators. Ecomorphological studies suggest that increased HEI tends to be associated with increased fossorial behaviors by helping generate power, force, and stability [4,5,24,27–31]. However, the relationship between HEI and sizes of the forearm flexors, pronators, and supinators remains largely untested.

Olecranon length index (OLI) = olecranon process length / ulna length. OLI estimates the relative mechanical advantage of the triceps brachii and dorsoepitrochlearis muscles used in

elbow extension. Biomechanical calculations indicates that an enlarged olecranon process facilitates stronger extension and flexion of the elbow and wrist by increasing mechanical advantage of these muscles, which in turn facilitate the ability to generate large forces [12]. Ecomorphological studies suggest that increased OLI is associated with increased fossoriality [4,5,24,27–31].

Ulnar robustness index (URI) = mediolateral diameter of ulna / ulna length. URI estimates the robustness of the ulna and its ability to resist bending and shearing stresses, and relative area available for the origin and insertion of forearm and manus flexors, pronators, and supinators. Performance studies on URI are limited. URI is presumably similar to radial robustness, where increased radial robustness is correlated with lower stresses at yield, lower elastic moduli, and higher resistance to failure when a bending force is applied [25]. Ecomorphological studies suggest that increased URI tends to be associated with fossorial and natatorial species whereas decreased URI tends to be associated with cursorial and scansorial species [5,24,26,27].

Manus proportions index (MAN) = metacarpal 3 length / humerus length. MAN estimates the relative proportions of proximal and distal elements of the forelimb, and relative size of the hand. Performance studies found that increased MAN is correlated with faster running speeds [23].

<u>Functional proxies for the hindlimb</u>

Crural index (CI) = tibia length / femur length. CI estimates relative proportions of proximal and distal elements of the hind limb. The relative longer distal end of the hindlimb facilitate increased stride length and decreased moment of inertia of limbs, which in turn

decreases the energetic cost of transport [14,17–22]. Performance studies found that increased CI is correlated with faster running speeds [23]. Ecomorphological studies suggest that increased CI tends to be associated with cursorial species whereas decreased CI tends to be associated with arboreal, natatorial, and fossorial species and [4,5,24].

Femoral robustness index (FRI) = anteroposterior diameter of femur / femur length. Estimates robustness of the femur and its ability to resist bending and shearing stresses. Performance studies found that increased FRI is correlated with lower stresses at yield, lower elastic moduli, and higher resistance to failure when a bending force is applied [25]. Ecomorphological studies suggest increased FRI tends to be associated with fossorial and natatorial species whereas decreased FRI tends to be associated with cursorial and scansorial species [5,24,26,27].

Gluteal index (GI) = length of distal extension of the greater trochanter of the femur / femur length. GI estimates the relative mechanical advantage of the gluteal muscles used in retraction of the femur. Ecomorphological studies suggest increased GI tends to be associated with fossorial [24]. However, empirical performance data investigating the functional advantages of increased GI remains largely untested.

Femoral epicondylar index (FEI) = epicondylar breadth of femur / femur length. FEI estimates the relative area available for the origins of the gastrocnemius and soleus muscles used in extension of the knee and plantar-flexion of the pes. Ecomorphological studies suggest that increased FEI tends to be associated with increased fossorial behaviors by helping generate power, force, and stability [4,5,24,27–31]. However, empirical performance data investigating the relationship between FEI and sizes of the gastrocnemius and soleus muscles remains largely untested.

Tibial robustness index (TRI) = mediolateral diameter of tibia / tibia length. TRI estimates robustness of the tibia and its ability to resist bending and shearing stresses. Performance studies found that increased TRI is correlated with lower stresses at yield, lower elastic moduli, and higher resistance to failure when a bending force is applied [25]. Ecomorphological studies suggest increased TRI tends to be associated with fossorial and natatorial species whereas decreased TRI tends to be associated with cursorial and scansorial species [5,24,26,27].

Pes length index (PES) = metatarsal 3 length / femur length. Estimates relative proportions of proximal and distal elements of the hind limb, and relative size of the hind foot. Performance studies found that increased PES is correlated with faster running speeds [19,23].

<u>Functional proxies for the vertebrae</u>

Because the carnivoran vertebral column can be divided into three regionalized modules (i.e., cervical, pre-diaphragmatic thoracic, and post-diaphragmatic thoracolumbar) with the diaphragmatic vertebra serving as a transitional vertebra [32], we only included the functional proxies of the fifth cervical vertebra, middle thoracic vertebra, diaphragmatic vertebra, and middle lumbar vertebra as our proxies for these four regions.

Sagittal second moment of area (sSMA) = $\pi/4$ * breadth of posterior centrum * height of the posterior centrum^3. sSMA estimates the stiffness in the of the vertebral joint in the sagittal plane. Biomechanical testing using cadaveric bending experiments found a strong correlation (r = 0.95) between sSMA and compliance (inverse of stiffness) [7].

Lateral second moment of area (lSMA) = $\pi/4$ * height of posterior centrum * breadth of the posterior centrum^3. lSMA estimates the stiffness in the of the vertebral joint in the lateral

plane. Biomechanical testing using cadaveric bending experiments found a strong correlation (r = 0.95) between sSMA and compliance (inverse of stiffness) [7].

Joint torsional angle (JTA) = 360º – absolute value of 270º – angle between postzygapophyses. JTA estimates the degree of axial torsion of the vertebrae. Biomechanical testing using cadaveric bending experiments found a strong correlation (r = 0.97) between JTA and mobility torsion of the vertebrae [7].

Joint verticality (JV) = absolute value of 180º – angle between postzygapophyses. JV estimates the relative importance of sagittal bending versus lateral bending of vertebral joints. Biomechanical testing using cadaveric bending experiments found a strong correlation (r = 0.77) between JV and the ratio of sagittal to lateral mobility of the vertebrae [7].

Ecological traits

We classified the 109 carnivoran species into one of seven locomotor regimes: arboreal (species that primarily live and forage in trees and rarely come down to the ground), cursorial (species that displays rapid bounding locomotion, particularly during hunting), scansorial (species that spend equal time in trees and on the ground), semi-aquatic (species that regularly swim for dispersal and/or foraging), semi-fossorial (species that regularly dig for shelter and/or foraging), and terrestrial (species that primarily live on the ground and rarely run, climb, dig, or swim during foraging). Terrestrial species were further categorized as terrestrial hunters (species that exhibit ambush and/or pouncing behaviors to kill prey) and terrestrial non-hunters (species that rarely hunt for prey). We also classified each species into one of seven dietary regimes: large prey hypercarnivory (consist of >70% terrestrial vertebrate prey that exceeds the predator's own body mass), medium prey hypercarnivory (consist of >70% terrestrial vertebrate prey that are up to the predator's own body mass), small prey hypercarnivory (consist of >70% terrestrial

vertebrate prey that are up to 20% of the predator's own body mass), omnivory (consist of >50% terrestrial vertebrates), insectivory (consisting of >70% invertebrates), aquatic carnivory (consist of >90% aquatic prey), and herbivory (consist of >90% plant material). Definitions for locomotor and dietary regimes were obtained from [33,34] with minor edits based on literature review.

Performance surfaces and adaptive landscapes

We investigated the functional optimality of the skeleton using adaptive landscape analyses [6,35–37]. All adaptive landscapes were computed using the R package Morphoscape [35]. We first created 27 performance surfaces by interpolating each of the 27 functional proxies across the morphospace surface using ordinary kriging. Each functional proxy was standardized and scaled from 0 to 1. We then computed a combined adaptive landscape (W) as the summation of all 27 performance surfaces (F_n), each weighted by their relative importance or contribution to overall fitness (w_n) [37]:

$$W = w_1F_1 + w_2F_2 + \bullet\bullet\bullet + w_nF_n$$

where W is optimized as the likelihood of combinations of performance surface and relative fitness, under the definition that the total fitness sums to 1 and the variance of all surfaces is equal [37]. We tested all possible combinations of weights, ranging from 0 to 1 in increments of 0.25, across a total of 27,405 possible adaptive landscapes (see Sensitivity Analyses section for further investigation of the concern with number of partition weight increments).

We identified the optimally weighted landscape that maximizes the fitness of each locomotor regime using the function calcWprimeBy, and tested whether these optimal landscapes are significantly different among locomotor ecological groups using the function multi.lands.grp.test. Significance testing for differences among landscapes was performed by

comparing the number of landscapes shared by the top 5% of each group with the total number of landscapes in the top 5% of models [6]. The top percentile of each group was determined using a chi-squared test. We also investigated differences in adaptive landscapes among dietary groups and carnivoran families that contained more than one species.

Sensitivity Analyses

Our adaptive landscape results may potentially be affected by (1) the size of the grid used to generate theoretical species, (2) the coarse increments of partition weights, (3) the use of functional proxies derived from theoretical species rather than data derived from actual species, and (4) removing the effects of size on the morphological traits in creating the morphospace. Therefore, we conducted a series of sensitivity analyses to investigate these potential problems.

Sensitivity Analyses 1: concern with number of theoretical species

We conducted sensitivity analyses to investigate whether the size of the grid used to generate theoretical species may potentially influence our adaptive landscape results. We increased our 9 x 7 grid size to 11 x 9 (generates 99 theoretical species) and 13 x 9 (generates 117 theoretical species). However, we found that the kriging procedure failed to generate a performance surface for a varying number of the functional proxies (Fig. S3). The cause of this failure is that NAs are being produced as values are being divided by 0, suggesting that these functional proxies have too small of a gradient to generate a performance surface during the kriging procedure. We view this phenomenon as a statistical artifact that affects the model fitting algorithms with no clear pattern as to which traits are being affected. Interestingly, it appears that there is no consistent pattern as to which functional proxies results in an incomplete performance

surface; most failed proxies do not fail in both 11 x 9 and 13 x 9 grids (Fig. S3). We suspect that, during the kriging procedure, the autofitVariogram function's automatic starting parameter may be arbitrarily chosen to initiate the interpolation. Another possibility is that this inconsistent pattern reflects the flatness of the krige surface of particular functional proxies under certain conditions of grid density.

Nevertheless, the remaining performance surfaces that were successfully generated in the larger 13 x 11 or 11 x 9 grid were identical to the performance surfaces when using the original 9 x 7 grid. Therefore, our sensitivity analyses indicate that the increasing sampling of theoretical species does not change the topological resolution of the performance surfaces. Furthermore, these errors in calculating the krige surface resulting in essentially flat performance surfaces support our concluding hypothesis that carnivorans occupy a broad adaptive zone relative to the overall mammalian adaptive landscape and thus exhibit a relatively flat landscape.

Sensitivity Analyses 2: concern with number of partition weight increments

We conducted sensitivity analyses to investigate whether the coarse increments of partition weights may potentially influence our adaptive landscape results. We reduced the number of functional indices by using linear discriminant analyses (LDA) to determine which set of functional proxies best separated out the species among locomotor groups. We conducted one LDA for the limb dataset and a second LDA for the vertebral dataset (see Table S7 for linear discriminant functions). We used LD1 (accounts for 44% of the variance in the limb dataset and 54%% of the variance in the vertebral dataset) to determine the top functional proxies to retain. In the first sensitivity analysis, we reduced the number of functional proxies to 14 by keeping both mandibular functional proxies (temMA and masMA), the top six vertebral functional

proxies (JTA and JV of the cervical, thoracic, and diaphragmatic vertebrae), and the top six limb functional proxies (HRI, HEI, OLI, FRI, FEI, and TRI). This enabled us to reduce the weight partition steps to 0.15, creating a total of 77,520 possible weight combinations. In the second sensitivity analysis, we kept only the top three (JTA and JV of the cervical and JV of the thoracic) vertebral functional proxies and top three limb functional proxies (HRI, HEI, and FRI), enabling us to reduce the weight partition steps to 0.05, creating a total of 53,130 possible weight combinations. We then used the same procedure described in the Supplementary Methods to create performance surfaces and optimized adaptive landscapes. Both sensitivity analyses revealed similar landscape topologies and optimized weights (Fig. S4; Table S8) with the analyses using all 27 functional proxies (Fig. 3). This suggests that the number of functional proxies and subsequent number of steps do not influence our results.

Sensitivity Analyses 3: concern with using functional proxies from theoretical species instead of actual species

We conducted sensitivity analyses to investigate whether the use of functional proxies derived from theoretical species rather than data derived from actual species may potentially influence our adaptive landscape results. We originally used theoretical grid values for building the landscape because specimen-specific values are always less evenly distributed in the morphospace than a grid. The unevenness contributes to heterogeneous resolution of the interpolation applied to the space by the ordinary kriging method, and thus unevenness in the landscape itself. Denser sampled regions will be more likely to have topological relief (i.e., peaks and valleys) than sparsely sampled regions when using actual specimen values, not necessarily because of a real underlying peak there. To demonstrate this, we conducted a sensitivity analysis

by creating performance surfaces and optimized adaptive landscapes using functional proxies measured from actual species. We found that the largest topological relief correspond with morphospace sample density; denser sampled regions exhibit more topological relief in performance surfaces and optimized adaptive landscapes (Fig. S5; Fig. S6). These topological features do not appear to be associated with locomotor ecologies; instead, clusters of species and even single species lie on top or bottom of topological peaks and valleys.

Sensitivity Analyses 4: concerns with removing the effects of size in creating the morphospace

We conducted sensitivity analyses to investigate whether removing the effects of size on the morphological traits in creating the morphospace may potentially influence our performance surfaces and adaptive landscape results. Although it is standard practice to remove the effects of size on morphology analyses, size may be an important predictor of functional performance across Carnivora. Terrestrial carnivorans exhibit a diverse range in body sizes from the 100 g least weasel to 800 kg polar bear. Size effects may therefore facilitate distinct ecological adaptations. We performed a PCA with the same 136 linear and angular measurements but with no size correcting to create the morphospace of the 109 terrestrial carnivoran species. We used the first two PC axes (PC 1 and PC 2 captured 92.4% and 0.02% of the variance, respectively) to create the morphospace (Fig. S7). We then used the same procedure described in the Supplementary Methods to create performance surfaces and optimized adaptive landscapes. We found that functional trade-offs and covariation patterns in the performance surfaces remain similar to the performance surfaces created using size-corrected traits (Fig. S8). The adaptive landscapes optimized by locomotion, diet, and family also exhibit similar topologies and optimized weights as the adaptive landscapes created using size-corrected traits (Fig. S9; Table S9–11).

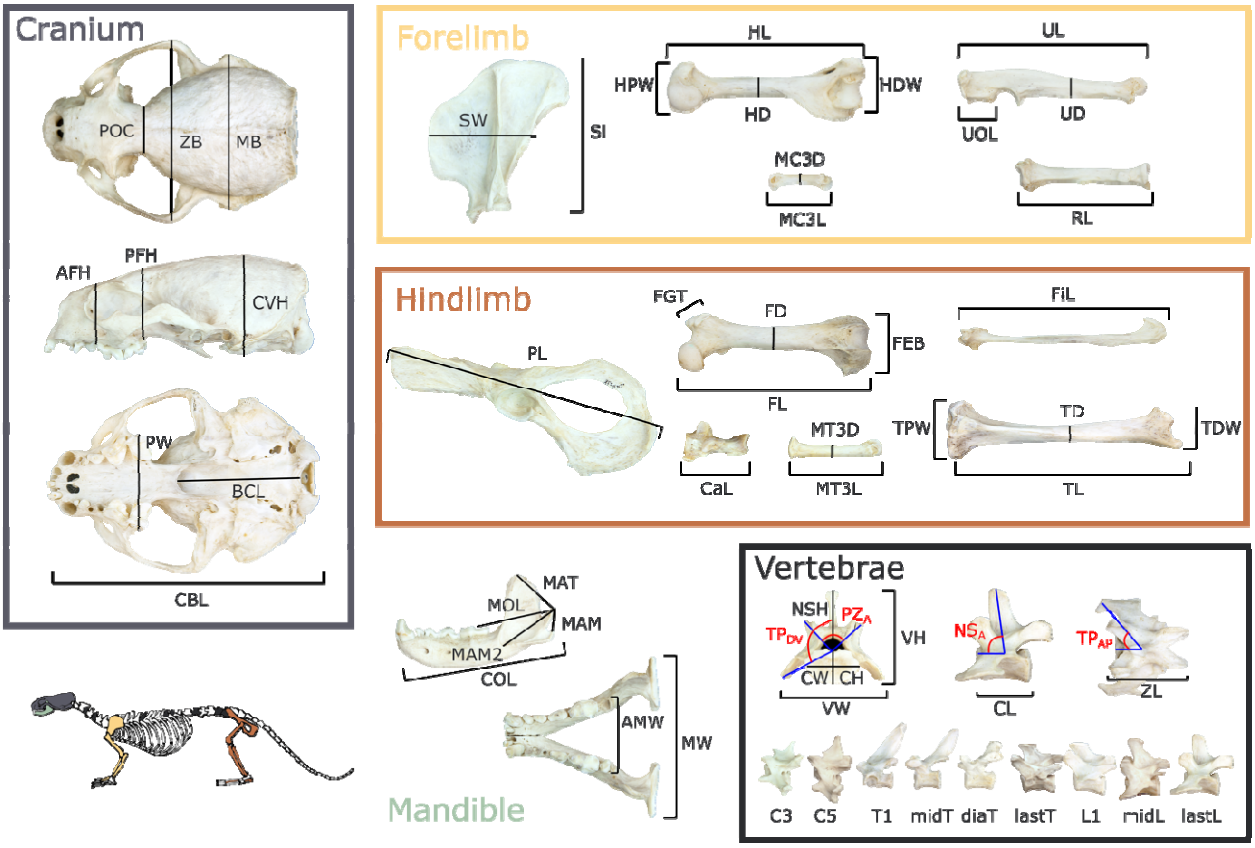

Fig. S1. Skeletal trait measurements used in this study. *Cranium*: CBL = condylobasal length, POC = postorbital constriction breadth, ZB = zygomatic breadth, MB = mastoid breadth, AFH = anterior facial height, PFH = posterior facial height, CVH = cranial vault height, PW = palate width, BCL = basicranial length. *Mandible*: MAT = moment arm of temporalis, MAM = moment arm of masseter, MAM2 = moment arm of masseter; MOL = molar out-lever; COL = canine out-lever; MW = mandibular width; AMW = anterior mandibular width. *Forelimb*: SL = scapula length; SW = scapula width; HL = humerus length; HD = humerus mid-shaft width; HPW = humerus proximal width; HDW = humerus distal width; UL = ulna length; UD = ulna mid-shaft width; UOL = ulnar olecranon length; RL = radius length; RD = radius mid-shaft width; MC3L = third metacarpel length; MC3W = third metacarpel width. *Hindlimb*: PL = pelvis length; FL = femur length; FD = femur mid-shaft width; FEB = femur distal width; FGT = height of the greater trochanter of the femur; TL = tibia length; TD = tibia mid-shaft width; TPW = tibia proximal width; TDW = tibia distal width; FiL = fibula length; CaL = calcaneus length; MT3L = third metatarsal length; MT3D = third metatarsal width. *Vertebrae*: VW = vertebrae width; VH = vertebrae height; CL = centrum length; CW = centrum width (posterior); CH = centrum height (posterior); ZL = inter-zygapophyseal length; NSH = neural spine height; TP_{DV} = transverse process dorsoventral projection; TP_{AP} = transverse process anteroposterior projection; PZ_A = angle between postzygapophyses; NSA_A = neural spine angle.

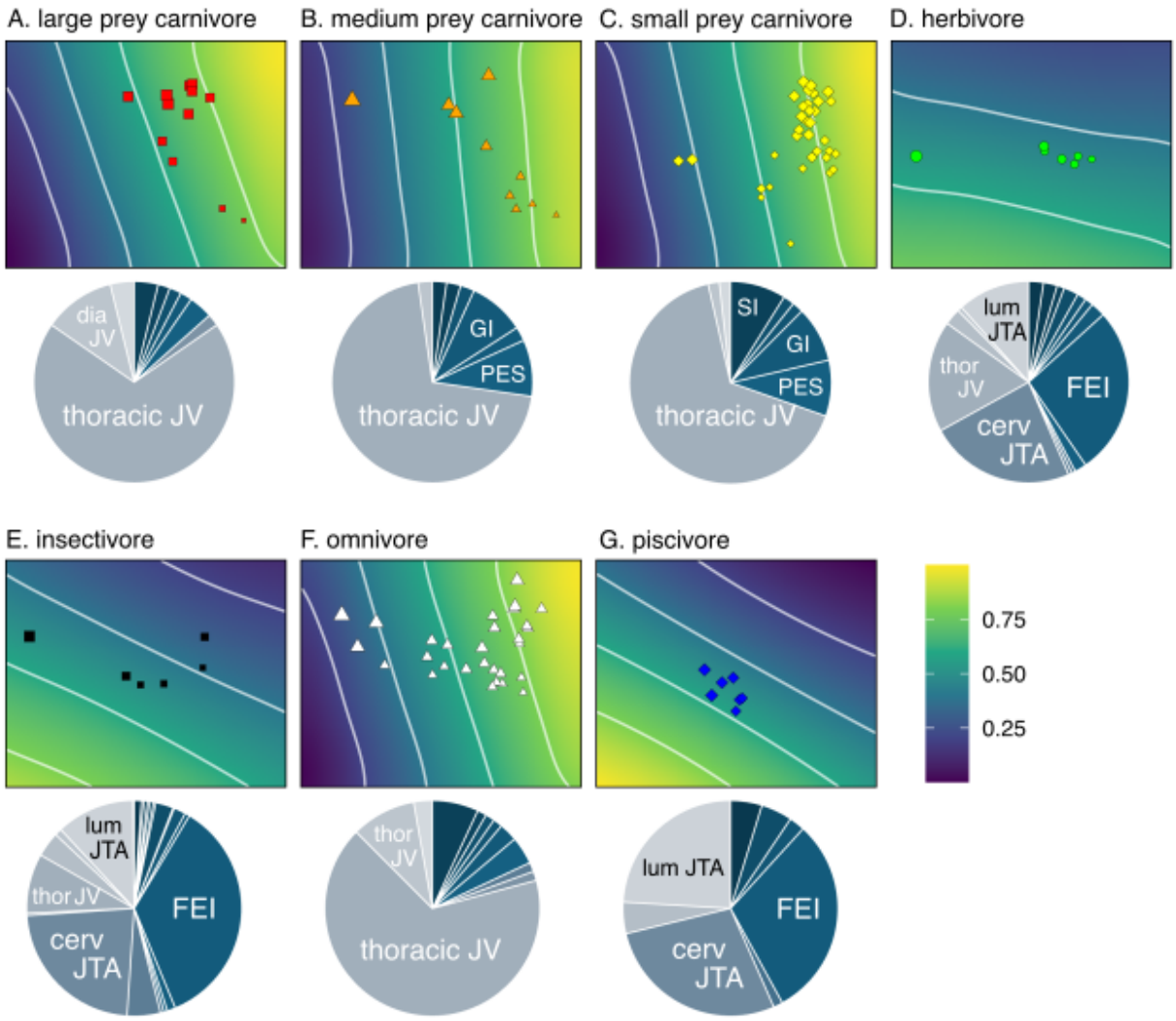

Fig. S2. Adaptive landscapes optimized for each dietary group. Adaptive landscapes were produced by combining the performance surfaces and optimizing their weightings to maximize the height of the landscape at the group mean. Pie charts show the relative weighting of each performance surface on each adaptive landscape (see Table S4 for full breakdown of optima weights). Functional indices with weights > 0.09 were labeled. Statistical tests comparing adaptive landscapes among dietary groups can be found in Table S3.

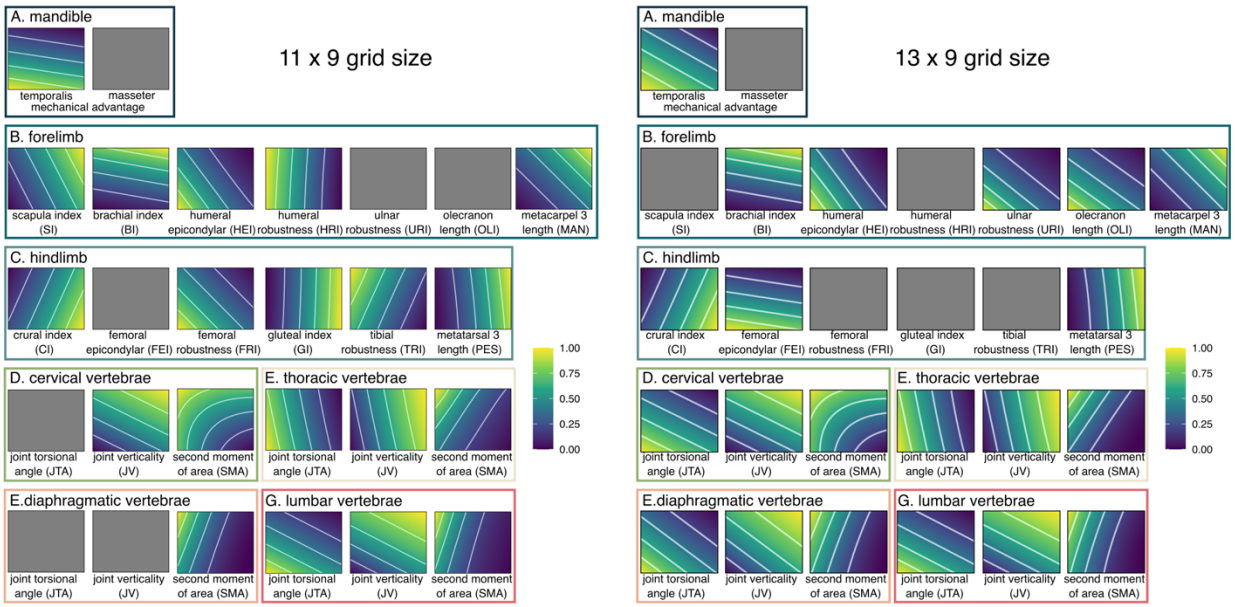

Fig. S3. Performance surfaces based on different grid sizes as part of Sensitivity Analyses 1, which investigated whether the size of the grid used to generate theoretical species may potentially influence our adaptive landscape results. Using larger grid sizes (i.e., 11 x 9 and 13 x 9) resulted in similar performance surfaces compared to the original 9 x 7 grid size, suggesting that increasing the number of theoretical species does not change the topology of performance surfaces. Gray squares indicate performance surfaces that failed to generate during the kriging procedure, likely because NAs are being produced as values are being divided by 0.

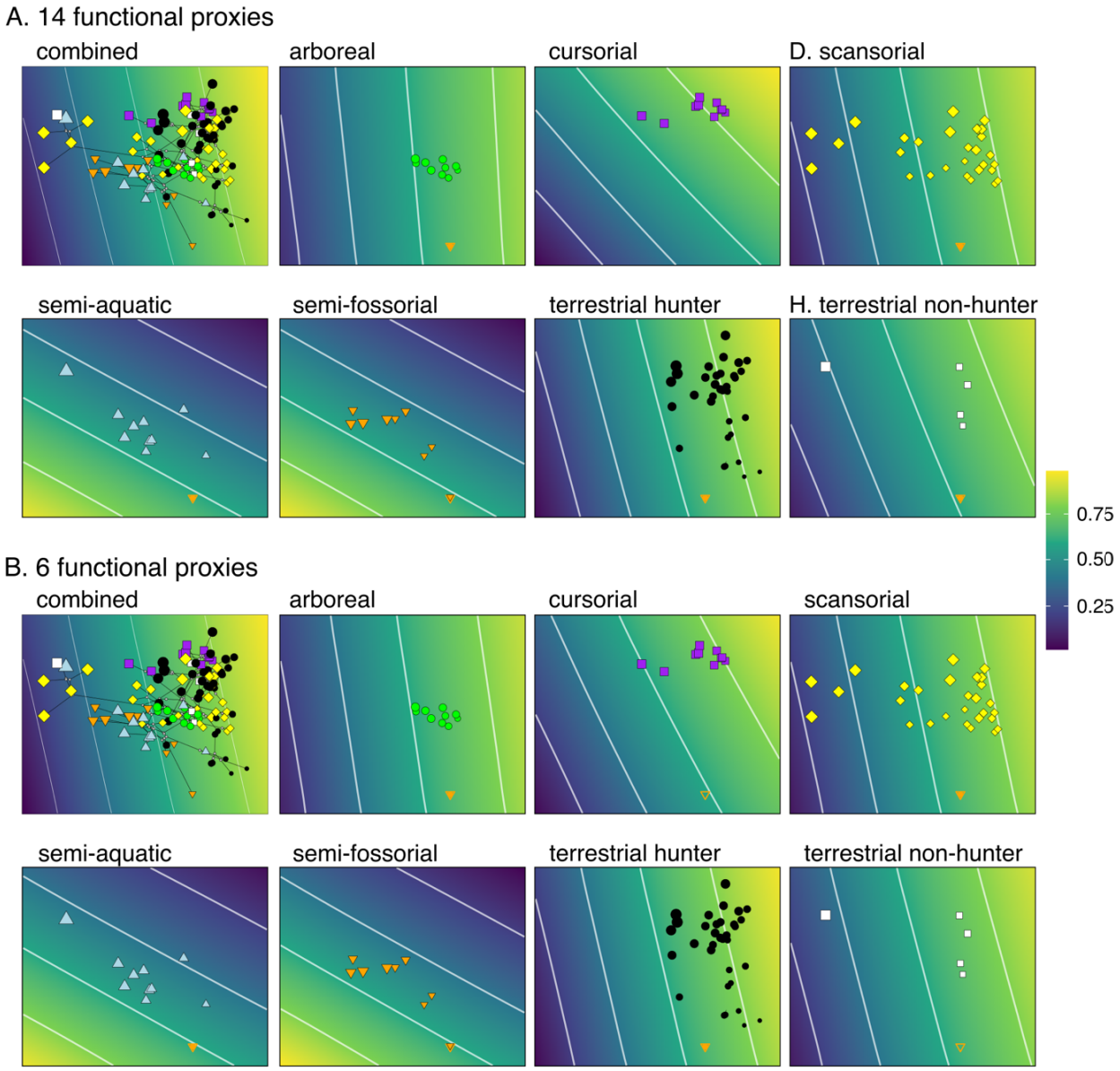

Fig. S4. Adaptive landscapes optimized for each locomotor group as part of Sensitivity Analyses 2, which investigated whether the coarse increments of partition weights may potentially influence our adaptive landscape results. Reducing the number of functional proxies from 27 to 14 (weight partition steps reduced to 0.15) or 6 (weight partition steps reduced to 0.07) does not change the topologies or weight partitions (Table S8) of the landscapes when optimized for each locomotor group. See Table S8 for breakdown of optima weights. See Figure 3 for original landscapes with all 27 functional proxies.

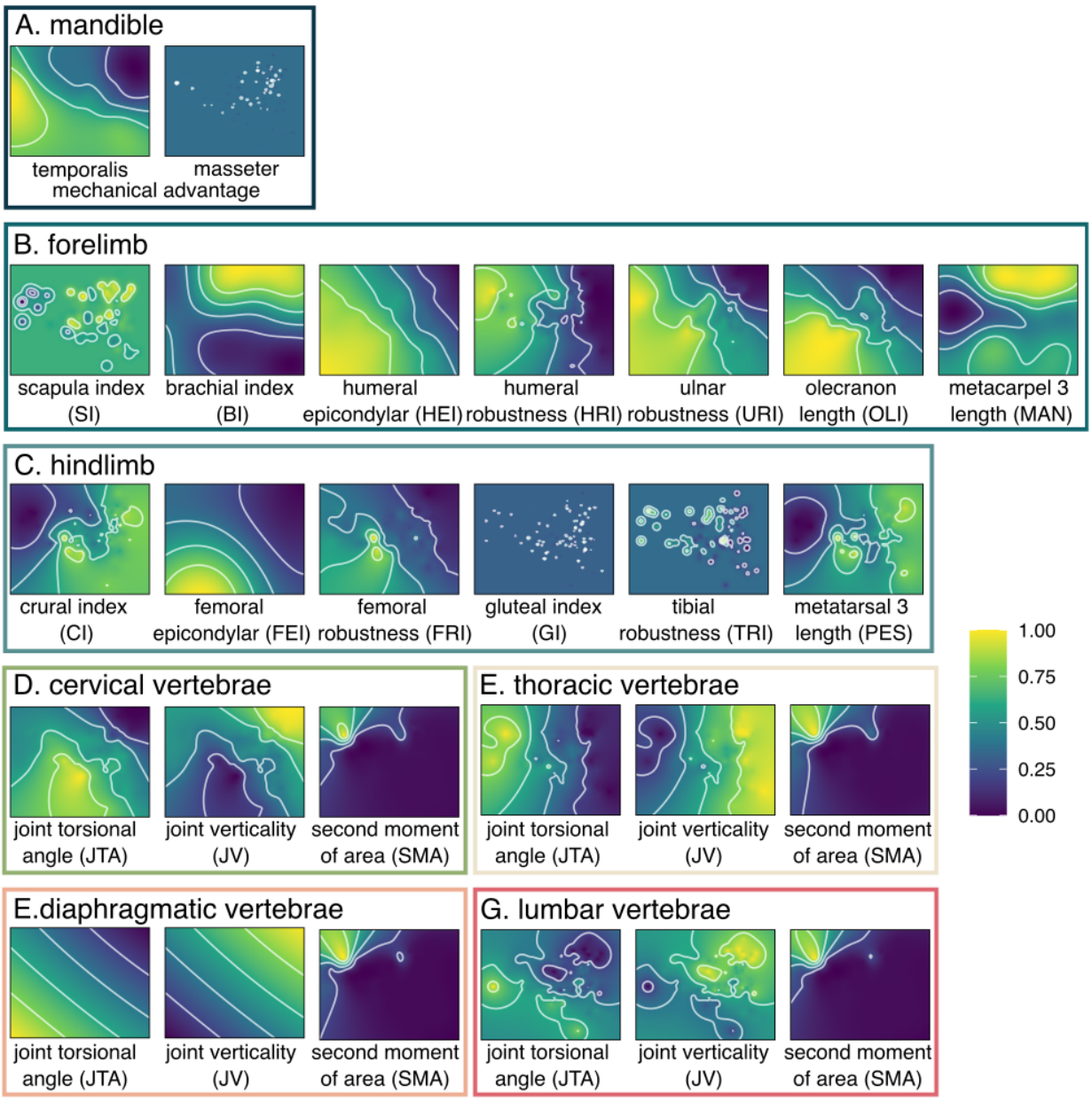

Fig. S5. Performance surfaces for each functional proxy based on empirical species data as part of Sensitivity Analyses 3, which investigated whether the use of functional proxies derived from theoretical species rather than data derived from actual species may potentially influence performance surfaces for each functional proxy. The largest topological relief correlates with morphospace sample density, suggesting that the unevenness contributes to heterogeneous resolution affect the topology of the performance surfaces. Color represents height on the performance surface.

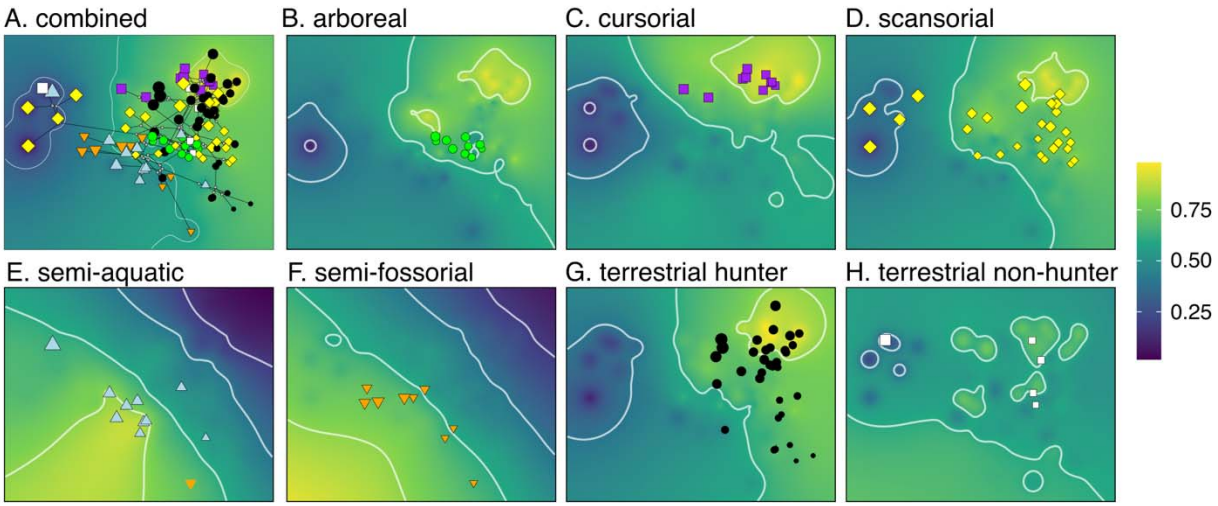

Fig. S6. Adaptive landscapes optimized for each locomotor group as part of Sensitivity Analyses 3, which investigated whether the use of functional proxies derived from theoretical species rather than data derived from actual species may potentially influence the optimized adaptive landscapes. The largest topological relief correlates with morphospace sample density, suggesting that the unevenness contributes to heterogeneous resolution affect the topology of the performance surfaces.

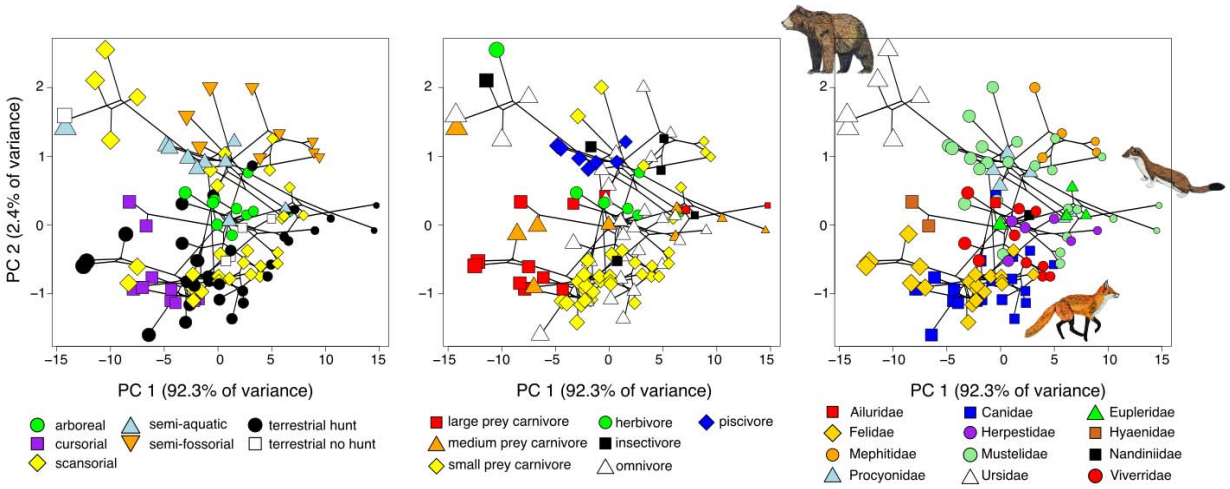

Fig. S7. Phylomorphospace of the carnivoran skeletal system defined by principal components (PCs) 1 and 2. PCA was conducted using 136 non-size corrected linear and angular measurements that capture morphological variation across the skull, appendicular, and axial skeletons. Size of points are scaled to estimated body size based on the geometric mean of all measurements.

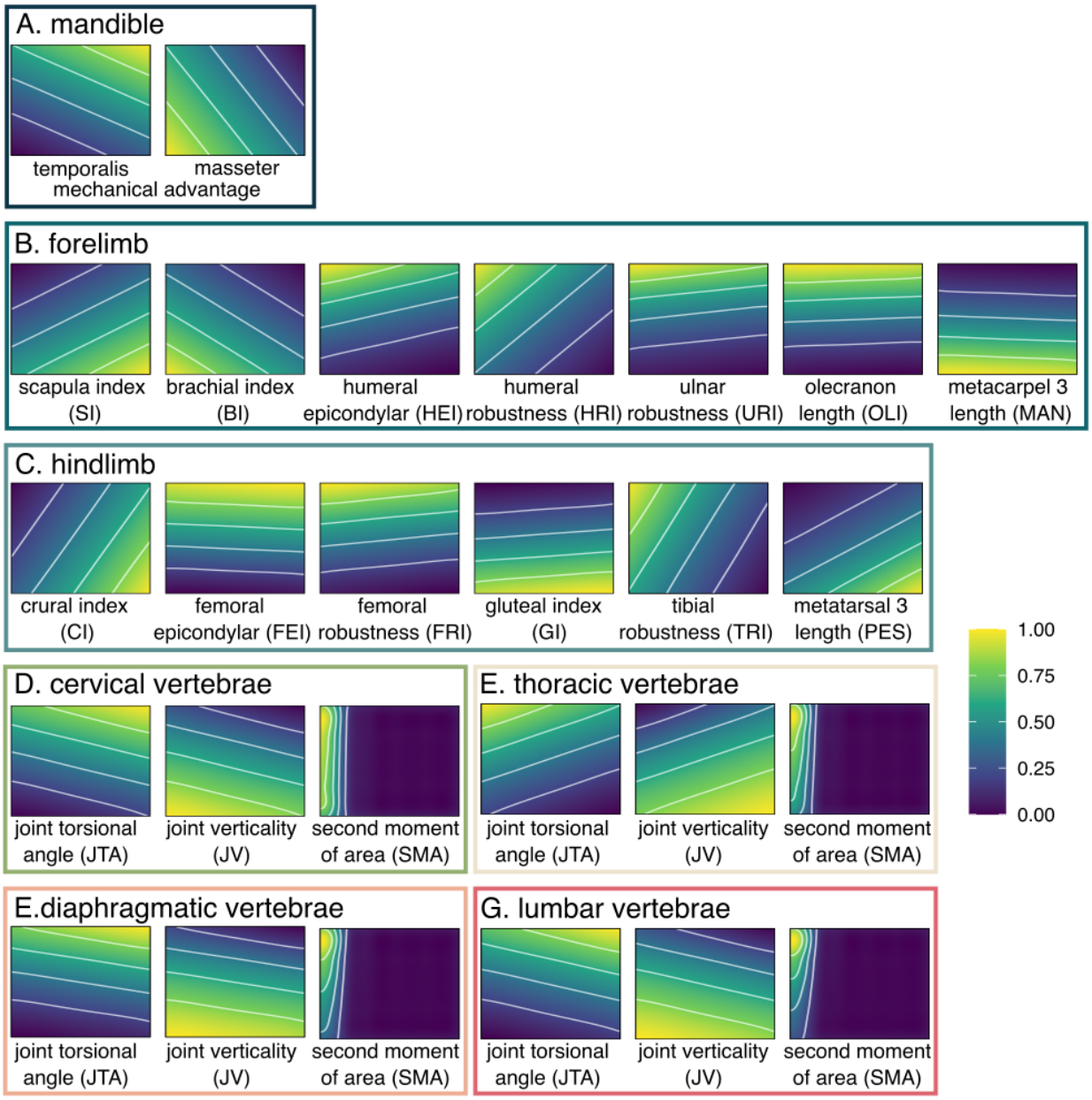

Fig. S8. Performance surfaces for each functional proxy based on non-size corrected morphological traits as part of Sensitivity Analyses 4, which investigated whether removing the effects of size on the morphological traits in creating the morphospace may potentially influence our performance surfaces and adaptive landscape results. The largest topological relief correlates with morphospace sample density, suggesting that the unevenness contributes to heterogeneous resolution affect the topology of the performance surfaces. Color represents height on the performance surface.

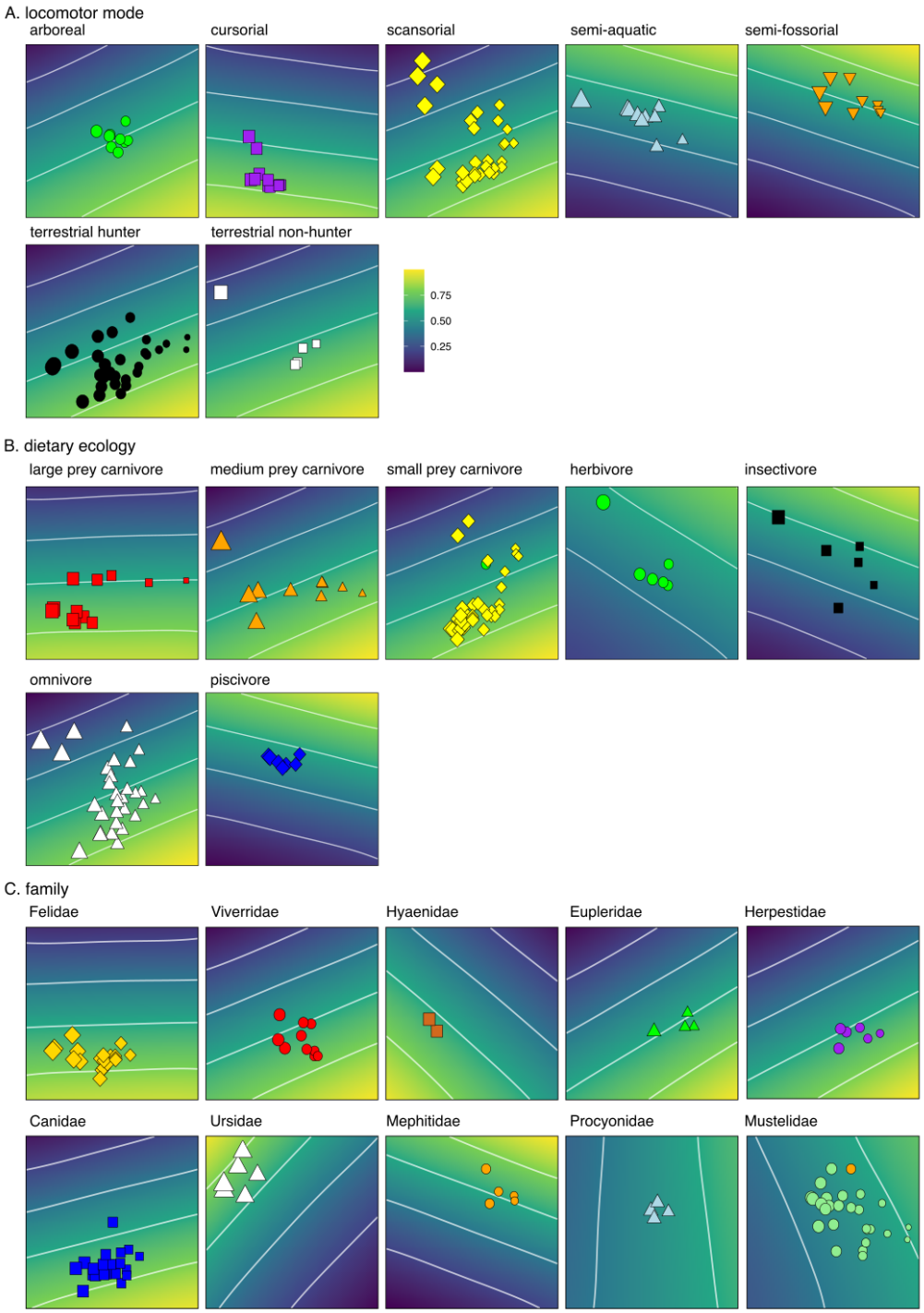

Fig. S9. Adaptive landscapes optimized for each locomotor, dietary, and familial groups as part of Sensitivity Analyses 4, which investigated whether removing the effects of size on the morphological traits in creating the morphospace may potentially influence our performance surfaces and adaptive landscape results. Using non-size corrected morphological traits does not change the topologies or weight partitions (Table S9–S11) of the landscapes when optimized for each locomotor group. See Tables S9–S11for breakdown of optima weights. See Figure 3 for original landscapes with all 27 functional proxies.

Table S1. PC loadings of skeletal traits. PC 1 and 2 explains 30.3% and 16.5% of the variance, respectively. Trait definitions are found in Figure S1.

trait	PC1	PC2
lnCBL	0.050	-0.058
lnPOC	0.039	0.005
lnZB	-0.001	-0.025
lnMB	-0.062	-0.183
lnCVH	0.028	-0.051
lnPW	0.074	-0.048
lnBCL	0.081	-0.078
lnMAT	0.000	-0.098
lnMAM	0.046	0.006
lnMAM2	0.028	0.009
lnMOL	0.017	0.021
lnCOL	0.070	0.025
lnMW	0.039	-0.088
lnAMW	0.033	-0.056
lnSL	0.007	0.143
lnSW	-0.056	0.111
lnHL	0.049	0.110
lnHD	-0.063	0.116
lnHPW	-0.052	0.042
lnHDW	-0.120	-0.015
lnUL	0.053	0.206
lnUD	-0.129	-0.020
lnUOL	-0.056	0.054
lnRL	0.075	0.256
lnRD	-0.060	0.248
lnMC3L	0.157	0.218
lnMC3W	-0.019	0.099
lnPL	-0.044	0.024
lnFL	0.059	0.143
lnFD	-0.043	0.044
lnFEB	-0.047	0.035
lnFGT	-0.135	0.047
lnTL	0.124	0.114
lnTD	0.023	0.159
lnTPW	-0.040	0.066
lnTDW	-0.053	0.050

lnFiL	0.130	0.118
lnCaL	0.033	0.100
lnMT3L	0.220	0.159
lnMT3D	0.038	0.123
lnC3_VW	-0.045	-0.087
lnC3_VH	0.042	-0.026
lnC3_CL	0.137	0.054
lnC3_CW	-0.055	-0.012
lnC3_CH	0.019	-0.008
lnC3_ZL	0.118	0.021
lnC3_NSH	0.057	-0.039
lnC3_TPDV	0.045	0.107
lnC3_PZA	-0.017	-0.067
lnC3_NSA	-0.002	-0.048
lnC3_TPAP	0.040	0.020
lnC5_VW	-0.081	-0.083
lnC5_VH	0.041	0.027
lnC5_CL	0.090	-0.017
lnC5_CW	-0.077	-0.054
lnC5_CH	0.034	0.054
lnC5_ZL	0.078	-0.024
lnC5_NSH	0.045	0.011
lnC5_TPDV	0.067	0.075
lnC5_PZA	-0.033	-0.067
lnC5_NSA	-0.044	-0.095
lnC5_TPAP	0.021	-0.003
lnT1_VW	-0.067	-0.062
lnT1_VH	0.020	0.099
lnT1_CL	0.062	-0.062
lnT1_CW	-0.072	0.022
lnT1_CH	-0.065	0.042
lnT1_ZL	0.051	-0.047
lnT1_NSH	0.040	0.111
lnT1_TPDV	0.165	0.051
lnT1_PZA	-0.057	-0.035
lnT1_NSA	-0.016	-0.010
lnT1_TPAP	-0.040	0.027
lnmidT_VW	-0.052	-0.050
lnmidT_VH	-0.040	0.129
lnmidT_CL	0.044	-0.120

lnmidT_CW	-0.053	0.010
lnmidT_CH	-0.082	0.086
lnmidT_ZL	0.013	-0.114
lnmidT_NSH	-0.027	0.142
lnmidT_TPDV	0.176	0.042
lnmidT_PZA	-0.118	-0.024
lnmidT_NSA	0.020	0.010
lnmidT_TPAP	-0.048	0.033
lntranT_VW	-0.052	-0.044
lntranT_VH	-0.113	0.074
lntranT_CL	0.058	-0.091
lntranT_CW	-0.060	0.000
lntranT_CH	-0.103	0.064
lntranT_ZL	-0.012	-0.096
lntranT_NSH	-0.117	0.076
lntranT_TPDV	0.142	0.086
lntranT_PZA	-0.089	-0.119
lntranT_NSA	0.014	0.032
lnlastT_VW	-0.071	-0.042
lnlastT_VH	-0.105	0.091
lnlastT_CL	0.079	-0.091
lnlastT_CW	-0.081	-0.001
lnlastT_CH	-0.114	0.039
lnlastT_ZL	0.046	-0.076
lnlastT_NSH	-0.101	0.118
lnlastT_PZA	-0.055	-0.150
lnlastT_NSA	-0.147	0.094
lnL1_VW	-0.085	0.077
lnL1_VH	-0.106	0.088
lnL1_CL	0.093	-0.079
lnL1_CW	-0.085	-0.003
lnL1_CH	-0.110	0.031
lnL1_ZL	0.055	-0.072
lnL1_NSH	-0.104	0.117
lnL1_TPDV	0.124	0.130
lnL1_PZA	-0.059	-0.126
lnL1_NSA	-0.160	0.095
lnL1_TPAP	-0.119	0.054
lnmidL_VW	-0.069	0.104
lnmidL_VH	-0.065	0.089

lnmidL_CL	0.128	-0.065
lnmidL_CW	-0.081	0.003
lnmidL_CH	-0.118	0.061
lnmidL_ZL	0.090	-0.086
lnmidL_NSH	-0.042	0.102
lnmidL_TPDV	0.140	0.107
lnmidL_PZA	-0.071	-0.137
lnmidL_NSA	-0.156	0.028
lnmidL_TPAP	-0.260	0.023
lnlastL_VW	-0.049	0.068
lnlastL_VH	-0.080	0.035
lnlastL_CL	0.079	-0.078
lnlastL_CW	-0.058	0.019
lnlastL_CH	-0.087	0.039
lnlastL_ZL	0.059	-0.100
lnlastL_NSH	-0.070	0.040
lnlastL_TPDV	0.155	-0.054
lnlastL_PZA	0.009	0.057
lnlastL_NSA	-0.130	0.011
lnlastL_TPAP	-0.207	-0.013

Table S2. Relative weights of each functional proxy optimized in the combined adaptive landscape across all carnivorans and optimized among the seven locomotor adaptive landscapes. The values represent the mean weights of the traits calculated from the top 5% of landscapes. Functional proxy definitions are found in Table 1.

functional proxies	combined	arboreal	cursorial	scansorial	semi-aquatic	semi-fossorial	terrestrial hunter	terrestrial non-hunter
temMA	0.00	0.00	0.00	0.00	0.03	0.03	0.00	0.00
masMA	0.02	0.03	0.00	0.01	0.00	0.00	0.00	0.00
SI	0.04	0.03	0.10	0.07	0.00	0.00	0.09	0.06
BI	0.02	0.00	0.15	0.01	0.00	0.00	0.00	0.07
HRI	0.00	0.00	0.00	0.00	0.00	0.00	0.00	0.00
HEI	0.00	0.00	0.00	0.00	0.00	0.00	0.00	0.00
OLI	0.00	0.00	0.00	0.00	0.09	0.09	0.00	0.00
MAN	0.02	0.00	0.10	0.01	0.00	0.00	0.02	0.02
CI	0.02	0.03	0.00	0.01	0.00	0.00	0.02	0.01
FRI	0.00	0.00	0.00	0.00	0.02	0.03	0.00	0.00
GI	0.04	0.03	0.03	0.07	0.00	0.00	0.09	0.03
FEI	0.00	0.03	0.00	0.00	0.25	0.25	0.00	0.00
TRI	0.00	0.00	0.00	0.00	0.00	0.00	0.00	0.00
PES	0.09	0.03	0.05	0.08	0.00	0.00	0.09	0.05
URI	0.00	0.00	0.00	0.00	0.05	0.05	0.00	0.00
$SMA_{cervical}$	0.00	0.00	0.00	0.00	0.00	0.00	0.00	0.00
$JTA_{cervical}$	0.00	0.03	0.00	0.00	0.25	0.25	0.00	0.00
$JV_{cervical}$	0.02	0.00	0.14	0.01	0.00	0.00	0.00	0.05
$SMA_{thoracic}$	0.00	0.00	0.00	0.00	0.00	0.00	0.00	0.00
$JTA_{thoracic}$	0.00	0.00	0.00	0.00	0.00	0.00	0.00	0.00
$JV_{thoracic}$	0.71	0.78	0.14	0.67	0.01	0.00	0.66	0.56
SMA_{dia}	0.00	0.00	0.00	0.00	0.00	0.00	0.00	0.00
JTA_{dia}	0.00	0.00	0.00	0.00	0.09	0.09	0.00	0.00
JV_{dia}	0.02	0.03	0.15	0.03	0.00	0.00	0.02	0.10
SMA_{lumbar}	0.00	0.00	0.00	0.00	0.00	0.00	0.00	0.00
JTA_{lumbar}	0.00	0.03	0.00	0.00	0.22	0.22	0.00	0.00
JV_{lumbar}	0.02	0.00	0.15	0.01	0.00	0.00	0.02	0.06
Z-score	0.69	0.69	0.80	0.68	0.70	0.76	0.81	0.63

Table S3. Pairwise significance tests among dietary adaptive landscapes. Top triangle: number of landscape models shared in the top 1% between the paired groups. Bottom triangle: P-values for difference between groups. Bolded P-values indicate significance.

	large prey carnivore	med prey carnivore	small prey carnivore	herbivore	insectivore	omnivore	piscivore
large prey carnivore	-	5	7	3	0	11	0
med prey carnivore	0.455	-	9	7	2	7	0
small prey carnivore	0.636	0.643	-	4	0	11	0
herbivore	0.273	0.500	0.286	-	196	4	63
insectivore	**0.001**	0.143	**0.001**	0.616	-	0	62
omnivore	1.000	0.500	0.786	**0.013**	**0.001**	-	0
piscivore	**0.001**	**0.001**	**0.001**	0.198	0.227	**0.001**	-

Table S4. Relative weights of each functional proxy optimized among the carnivoran familial adaptive landscapes. The values represent the mean weights of the traits calculated from the top 5% of landscapes. Functional proxy definitions are found in Table 1.

functional proxies	Nand	Feli	Vive	Hyae	Eupl	Herp	Cani	Ursi	Meph	Ailu	Proc	Must
temMA	0.00	0.00	0.00	0.00	0.00	0.00	0.00	0.00	0.03	0.02	0.00	0.08
masMA	0.04	0.00	0.02	0.00	0.03	0.03	0.00	0.00	0.00	0.02	0.02	0.06
SI	0.04	0.09	0.05	0.00	0.03	0.03	0.14	0.00	0.00	0.02	0.02	0.00
BI	0.00	0.02	0.00	0.33	0.00	0.00	0.03	0.00	0.00	0.00	0.02	0.00
HRI	0.00	0.00	0.00	0.00	0.00	0.00	0.00	0.16	0.00	0.00	0.00	0.00
HEI	0.00	0.00	0.00	0.00	0.00	0.00	0.00	0.01	0.00	0.00	0.00	0.00
OLI	0.00	0.00	0.00	0.00	0.00	0.00	0.00	0.00	0.08	0.02	0.02	0.03
MAN	0.00	0.04	0.00	0.00	0.00	0.00	0.06	0.00	0.00	0.00	0.00	0.00
CI	0.04	0.00	0.02	0.00	0.03	0.03	0.00	0.00	0.00	0.02	0.02	0.03
FRI	0.00	0.00	0.00	0.00	0.00	0.00	0.00	0.01	0.02	0.00	0.00	0.00
GI	0.04	0.02	0.09	0.00	0.09	0.10	0.02	0.00	0.00	0.02	0.02	0.02
FEI	0.00	0.00	0.00	0.00	0.00	0.00	0.00	0.01	0.26	0.06	0.02	0.20
TRI	0.00	0.00	0.00	0.03	0.00	0.00	0.00	0.19	0.00	0.00	0.00	0.00
PES	0.04	0.06	0.11	0.00	0.03	0.10	0.05	0.00	0.00	0.02	0.02	0.02
URI	0.00	0.00	0.00	0.00	0.00	0.00	0.00	0.00	0.04	0.00	0.00	0.01
$SMA_{cervical}$	0.00	0.00	0.00	0.39	0.00	0.00	0.00	0.24	0.00	0.00	0.02	0.00
$JTA_{cervical}$	0.00	0.00	0.00	0.00	0.00	0.00	0.00	0.00	0.26	0.06	0.02	0.22
$JV_{cervical}$	0.00	0.05	0.00	0.07	0.00	0.00	0.07	0.00	0.00	0.00	0.02	0.00
$SMA_{thoracic}$	0.00	0.00	0.00	0.00	0.00	0.00	0.00	0.13	0.00	0.00	0.00	0.00
$JTA_{thoracic}$	0.00	0.00	0.00	0.00	0.00	0.00	0.00	0.08	0.00	0.00	0.00	0.00
$JV_{thoracic}$	0.79	0.55	0.68	0.03	0.75	0.70	0.36	0.00	0.01	0.72	0.77	0.12
SMA_{dia}	0.00	0.00	0.00	0.00	0.00	0.00	0.00	0.10	0.00	0.00	0.00	0.00
JTA_{dia}	0.00	0.00	0.00	0.00	0.00	0.00	0.00	0.01	0.08	0.02	0.02	0.03
JV_{dia}	0.04	0.11	0.02	0.05	0.03	0.03	0.17	0.00	0.00	0.02	0.02	0.00
SMA_{lumbar}	0.00	0.00	0.00	0.00	0.00	0.00	0.00	0.07	0.00	0.00	0.00	0.00
JTA_{lumbar}	0.00	0.00	0.00	0.00	0.00	0.00	0.00	0.00	0.21	0.02	0.02	0.18
JV_{lumbar}	0.00	0.06	0.00	0.10	0.00	0.00	0.10	0.00	0.00	0.00	0.02	0.00
Z-score	0.73	0.81	0.78	0.69	0.74	0.78	0.83	0.89	0.70	0.66	0.62	0.68

Table S5. Relative weights of each functional proxy optimized among the dietary adaptive landscapes. The values represent the mean weights of the traits calculated from the top 5% of landscapes. Functional proxy definitions are found in Table 1.

functional proxies	large prey carnivore	med prey carnivore	small prey carnivore	herbivore	insectivore	omnivore	piscivore
temMA	0.00	0.00	0.00	0.03	0.01	0.00	0.03
masMA	0.00	0.02	0.00	0.02	0.00	0.00	0.00
SI	0.05	0.02	0.09	0.01	0.00	0.08	0.00
BI	0.02	0.00	0.00	0.00	0.01	0.01	0.00
HRI	0.00	0.00	0.00	0.00	0.01	0.00	0.00
HEI	0.00	0.00	0.00	0.00	0.00	0.00	0.00
OLI	0.00	0.00	0.00	0.06	0.07	0.00	0.09
MAN	0.02	0.00	0.02	0.00	0.00	0.01	0.00
CI	0.00	0.05	0.02	0.02	0.00	0.01	0.00
FRI	0.00	0.00	0.00	0.01	0.02	0.00	0.03
GI	0.02	0.09	0.09	0.02	0.01	0.03	0.00
FEI	0.00	0.02	0.00	0.20	0.23	0.00	0.25
TRI	0.00	0.00	0.00	0.00	0.01	0.00	0.00
PES	0.02	0.09	0.09	0.02	0.00	0.07	0.00
URI	0.00	0.00	0.00	0.03	0.04	0.00	0.05
$SMA_{cervical}$	0.00	0.00	0.00	0.01	0.07	0.01	0.00
$JTA_{cervical}$	0.00	0.02	0.00	0.20	0.20	0.00	0.25
$JV_{cervical}$	0.02	0.00	0.00	0.00	0.00	0.01	0.00
$SMA_{thoracic}$	0.00	0.00	0.00	0.00	0.00	0.00	0.00
$JTA_{thoracic}$	0.00	0.00	0.00	0.00	0.00	0.00	0.00
$JV_{thoracic}$	0.73	0.68	0.66	0.15	0.08	0.67	0.00
SMA_{dia}	0.00	0.00	0.00	0.00	0.00	0.00	0.00
JTA_{dia}	0.00	0.00	0.00	0.06	0.07	0.00	0.09
JV_{dia}	0.09	0.02	0.02	0.00	0.00	0.07	0.00
SMA_{lumbar}	0.00	0.00	0.00	0.00	0.00	0.00	0.00
JTA_{lumbar}	0.00	0.00	0.00	0.16	0.15	0.00	0.22
JV_{lumbar}	0.02	0.00	0.02	0.00	0.00	0.01	0.00
Z-score	0.72	0.70	0.79	0.59	0.57	0.68	0.75

Table S6. Pairwise significance tests among familial adaptive landscapes. Top triangle: number of landscape models shared in the top 1% between the paired groups. Bottom triangle: P-values for difference between groups. Bolded P-values indicate significance.

	Nand	Feli	Vive	Hyae	Eupl	Herp	Cani	Ursi	Meph	Ailu	Proc	Must
Nand	-	5	7	0	7	7	5	0	0	7	7	1
Feli	0.714	-	7	0	5	6	35	0	0	5	8	1
Vive	1.000	0.200	-	0	8	10	7	0	0	7	7	1
Hyae	**0.001**	**0.001**	**0.001**	-	0	0	0	0	0	0	0	0
Eupl	1.000	0.143	0.727	**0.001**	-	8	5	0	0	7	7	1
Herp	1.000	0.171	0.909	**0.001**	1.000	-	6	0	0	7	7	1
Cani	0.714	1.000	0.636	**0.001**	0.625	0.600	-	0	0	5	8	1
Ursi	**0.001**	**0.001**	**0.001**	0.059	**0.001**	**0.001**	**0.001**	-	0	0	0	0
Meph	**0.001**	**0.001**	**0.001**	**0.001**	**0.001**	**0.001**	**0.001**	**0.001**	-	0	0	58
Ailu	1.000	0.143	0.636	**0.001**	0.875	0.700	0.053	**0.001**	**0.001**	-	12	8
Proc	1.000	0.229	0.636	**0.001**	0.875	0.700	0.084	**0.001**	**0.001**	0.750	-	4
Must	0.143	**0.029**	0.091	**0.001**	0.125	0.100	**0.011**	**0.001**	0.630	0.500	0.267	-

Table S7. Scaling matrix for the first linear discriminant function (LD1). Separate LDAs were performed for the limb and vertebral datasets.

functional proxies	LD1
limbs	
BI	3.307
CI	3.268
FEI	11.948
FRI	20.308
GI	0.690
HEI	33.182
HRI	-83.410
IM	0.474
MANUS	-0.506
OLI	10.067
PES	3.282
SI	-0.675
TRI	5.948
URI	-5.670
vertebrae	
$JTA_{cervical}$	-0.052
$JV_{cervical}$	0.052
Lateral $SMA_{cervical}$	0.000
Sagittal $SMA_{cervical}$	0.000
JTA_{lumbar}	-0.004
JV_{lumbar}	0.004
Lateral SMA_{lumbar}	0.000
Sagittal SMA_{lumbar}	0.000
$JTA_{thoracic}$	-0.013
$JV_{thoracic}$	0.013
Lateral $SMA_{thoracic}$	0.000
Sagittal $SMA_{thoracic}$	0.000
JTA_{dia}	-0.013
JV_{dia}	0.013
Lateral SMA_{dia}	0.000
Sagittal SMA_{dia}	0.000

Table S8. Relative weights of each functional proxy optimized among the seven locomotor adaptive landscapes from Sensitivity Analyses 2, which investigated whether the coarse increments of partition weights may potentially influence our adaptive landscape results. (**A)** Relative weights of proxies when the number of proxies was reduced to 14 and incremental weight partitions was reduced to 0.15. (**B)** Relative weights of proxies when the number of proxies was reduced to 6 and incremental weight partitions was reduced to 0.07. The values represent the mean weights of the traits calculated from the top 5% of landscapes.

functional proxies	arboreal	cursorial	scansorial	semi-aquatic	semi-fossorial	terrestrial hunter	terrestrial non-hunter
A. number of proxies reduced to 14							
temMA	0.01	0.00	0.01	0.03	0.04	0.00	0.00
masMA	0.04	0.00	0.02	0.01	0.01	0.03	0.01
HRI	0.00	0.00	0.00	0.01	0.00	0.00	0.01
HEI	0.00	0.00	0.00	0.01	0.01	0.00	0.00
OLI	0.01	0.00	0.01	0.05	0.06	0.00	0.00
FRI	0.01	0.00	0.00	0.03	0.03	0.00	0.00
FEI	0.04	0.00	0.02	0.43	0.42	0.00	0.02
TRI	0.00	0.00	0.00	0.01	0.00	0.00	0.01
$JTA_{cervical}$	0.04	0.00	0.02	0.35	0.36	0.00	0.01
$JV_{cervical}$	0.01	0.33	0.02	0.00	0.00	0.03	0.06
$JTA_{thoracic}$	0.00	0.00	0.00	0.01	0.01	0.00	0.00
$JV_{thoracic}$	0.79	0.33	0.80	0.02	0.01	0.86	0.64
JTA_{dia}	0.01	0.00	0.01	0.06	0.06	0.00	0.01
JV_{dia}	0.04	0.33	0.10	0.00	0.00	0.09	0.21
Z	0.69	0.82	0.69	0.69	0.75	0.83	0.64
B. number of proxies reduced to 6							
HRI	0.01	0.01	0.01	0.02	0.02	0.01	0.02
HEI	0.01	0.00	0.01	0.03	0.03	0.01	0.01
FRI	0.02	0.01	0.01	0.07	0.06	0.01	0.02
$JTA_{cervical}$	0.06	0.01	0.04	0.81	0.84	0.01	0.03
$JV_{cervical}$	0.02	0.30	0.05	0.01	0.00	0.05	0.09
$JTA_{thoracic}$	0.01	0.01	0.01	0.02	0.02	0.01	0.02
$JV_{thoracic}$	0.87	0.66	0.87	0.04	0.02	0.91	0.82
Z	0.69	0.79	0.69	0.68	0.74	0.81	0.64

Table S9. Relative weights of each functional proxy optimized among the seven locomotor adaptive landscapes from Sensitivity Analyses 4, which investigated whether removing the effects of size on the morphological traits in creating the morphospace may potentially influence the optimized weights of the adaptive landscape. The values represent the mean weights of the traits calculated from the top 5% of landscapes.

functional proxies	arboreal	cursorial	scansorial	semi-aquatic	semi-fossorial	terrestrial hunter	terrestrial non-hunter
temMA	0.02	0.00	0.00	0.19	0.30	0.00	0.00
masMA	0.00	0.10	0.00	0.00	0.00	0.00	0.01
SI	0.09	0.05	0.18	0.00	0.00	0.21	0.13
BI	0.00	0.07	0.00	0.00	0.00	0.00	0.00
HRI	0.00	0.00	0.00	0.01	0.00	0.00	0.00
HEI	0.00	0.00	0.00	0.00	0.00	0.00	0.00
OLI	0.00	0.00	0.00	0.03	0.00	0.00	0.00
MAN	0.00	0.07	0.01	0.00	0.00	0.01	0.01
CI	0.02	0.00	0.01	0.00	0.00	0.00	0.01
FRI	0.00	0.00	0.00	0.02	0.00	0.00	0.00
GI	0.02	0.11	0.03	0.00	0.00	0.04	0.03
FEI	0.00	0.00	0.00	0.15	0.07	0.00	0.00
TRI	0.00	0.00	0.00	0.03	0.00	0.00	0.00
PES	0.05	0.02	0.07	0.00	0.00	0.09	0.07
URI	0.00	0.00	0.00	0.00	0.00	0.00	0.00
$SMA_{cervical}$	0.00	0.00	0.00	0.00	0.00	0.00	0.00
$JTA_{cervical}$	0.02	0.00	0.00	0.25	0.28	0.00	0.00
$JV_{cervical}$	0.00	0.13	0.01	0.00	0.00	0.01	0.01
$SMA_{thoracic}$	0.00	0.00	0.00	0.00	0.00	0.00	0.00
$JTA_{thoracic}$	0.00	0.00	0.00	0.00	0.00	0.00	0.00
$JV_{thoracic}$	0.73	0.16	0.62	0.05	0.00	0.57	0.63
SMA_{dia}	0.00	0.00	0.00	0.00	0.00	0.00	0.00
JTA_{dia}	0.00	0.00	0.00	0.10	0.10	0.00	0.00
JV_{dia}	0.02	0.16	0.03	0.00	0.00	0.04	0.07
SMA_{lumbar}	0.00	0.00	0.00	0.00	0.00	0.00	0.00
JTA_{lumbar}	0.00	0.00	0.00	0.16	0.25	0.00	0.00
JV_{lumbar}	0.02	0.15	0.03	0.00	0.00	0.03	0.03
Z-score	0.68	0.80	0.69	0.60	0.82	0.81	0.65

Table S10. Relative weights of each functional proxy optimized among the seven dietary adaptive landscapes from Sensitivity Analyses 4, which investigated whether removing the effects of size on the morphological traits in creating the morphospace may potentially influence the optimized weights of the adaptive landscape. The values represent the mean weights of the traits calculated from the top 5% of landscapes.

functional proxies	large prey carnivore	med prey carnivore	small prey carnivore	herbivore	insectivore	omnivore	piscivore
temMA	0.00	0.00	0.00	0.19	0.26	0.00	0.19
masMA	0.08	0.00	0.00	0.00	0.00	0.00	0.00
SI	0.04	0.15	0.22	0.06	0.02	0.17	0.00
BI	0.02	0.00	0.00	0.00	0.00	0.00	0.00
HRI	0.00	0.00	0.00	0.00	0.00	0.00	0.00
HEI	0.00	0.00	0.00	0.00	0.00	0.00	0.00
OLI	0.00	0.00	0.00	0.02	0.02	0.00	0.03
MAN	0.02	0.00	0.01	0.00	0.00	0.02	0.00
CI	0.00	0.02	0.00	0.02	0.01	0.02	0.00
FRI	0.00	0.00	0.00	0.01	0.01	0.00	0.03
GI	0.04	0.02	0.04	0.01	0.00	0.03	0.00
FEI	0.00	0.00	0.00	0.09	0.10	0.00	0.15
TRI	0.00	0.00	0.00	0.01	0.00	0.00	0.01
PES	0.01	0.08	0.09	0.03	0.01	0.08	0.00
URI	0.00	0.00	0.00	0.00	0.00	0.00	0.00
$SMA_{cervical}$	0.00	0.00	0.00	0.00	0.00	0.00	0.00
$JTA_{cervical}$	0.00	0.00	0.00	0.19	0.25	0.00	0.27
$JV_{cervical}$	0.06	0.02	0.01	0.00	0.00	0.02	0.00
$SMA_{thoracic}$	0.00	0.00	0.00	0.00	0.00	0.00	0.00
$JTA_{thoracic}$	0.00	0.00	0.00	0.00	0.00	0.00	0.00
$JV_{thoracic}$	0.43	0.65	0.57	0.16	0.06	0.63	0.01
SMA_{dia}	0.00	0.00	0.00	0.00	0.00	0.00	0.00
JTA_{dia}	0.00	0.00	0.00	0.08	0.10	0.00	0.12
JV_{dia}	0.19	0.04	0.03	0.01	0.00	0.03	0.00
SMA_{lumbar}	0.00	0.00	0.00	0.00	0.00	0.00	0.00
JTA_{lumbar}	0.00	0.00	0.00	0.12	0.17	0.00	0.17
JV_{lumbar}	0.11	0.02	0.01	0.00	0.00	0.02	0.00
Z-score	0.72	0.70	0.79	0.57	0.63	0.69	0.64

Table S11. Relative weights of each functional proxy optimized among the familial adaptive landscapes from Sensitivity Analyses 4, which investigated whether removing the effects of size on the morphological traits in creating the morphospace may potentially influence the optimized weights of the adaptive landscape. The values represent the mean weights of the traits calculated from the top 5% of landscapes.

functional proxies	Feli	Vive	Hyae	Eupl	Herp	Cani	Ursi	Meph	Proc	Must
temMA	0.00	0.00	0.00	0.02	0.00	0.00	0.00	0.41	0.23	0.21
masMA	0.02	0.00	0.66	0.00	0.00	0.00	0.00	0.00	0.00	0.00
SI	0.07	0.18	0.00	0.27	0.30	0.13	0.00	0.00	0.09	0.11
BI	0.02	0.00	0.02	0.00	0.00	0.01	0.00	0.00	0.00	0.00
HRI	0.00	0.00	0.00	0.00	0.00	0.00	0.23	0.00	0.00	0.00
HEI	0.00	0.00	0.00	0.00	0.00	0.00	0.02	0.00	0.00	0.00
OLI	0.00	0.00	0.00	0.00	0.00	0.00	0.02	0.00	0.00	0.00
MAN	0.04	0.00	0.00	0.00	0.00	0.03	0.00	0.00	0.00	0.00
CI	0.00	0.02	0.00	0.09	0.03	0.00	0.00	0.00	0.03	0.05
FRI	0.00	0.00	0.00	0.00	0.00	0.00	0.02	0.00	0.00	0.00
GI	0.09	0.03	0.02	0.00	0.02	0.08	0.00	0.00	0.00	0.01
FEI	0.00	0.00	0.00	0.00	0.00	0.00	0.03	0.03	0.03	0.04
TRI	0.00	0.00	0.02	0.00	0.00	0.00	0.57	0.00	0.00	0.00
PES	0.02	0.08	0.00	0.13	0.13	0.06	0.00	0.00	0.03	0.06
URI	0.00	0.00	0.00	0.00	0.00	0.00	0.01	0.00	0.00	0.00
$SMA_{cervical}$	0.00	0.00	0.00	0.00	0.00	0.00	0.00	0.00	0.00	0.00
$JTA_{cervical}$	0.00	0.00	0.00	0.00	0.00	0.00	0.02	0.30	0.14	0.16
$JV_{cervical}$	0.09	0.02	0.02	0.00	0.00	0.03	0.00	0.00	0.00	0.00
$SMA_{thoracic}$	0.00	0.00	0.00	0.00	0.00	0.00	0.00	0.00	0.00	0.00
$JTA_{thoracic}$	0.00	0.00	0.00	0.00	0.00	0.00	0.03	0.00	0.00	0.00
$JV_{thoracic}$	0.31	0.62	0.09	0.50	0.50	0.50	0.00	0.00	0.36	0.22
SMA_{dia}	0.00	0.00	0.00	0.00	0.00	0.00	0.00	0.00	0.00	0.00
JTA_{dia}	0.00	0.00	0.00	0.00	0.00	0.00	0.02	0.05	0.02	0.05
JV_{dia}	0.20	0.03	0.09	0.00	0.02	0.10	0.00	0.00	0.00	0.00
SMA_{lumbar}	0.00	0.00	0.00	0.00	0.00	0.00	0.00	0.00	0.00	0.00
JTA_{lumbar}	0.00	0.00	0.00	0.00	0.00	0.00	0.02	0.21	0.06	0.10
JV_{lumbar}	0.15	0.02	0.09	0.00	0.00	0.06	0.00	0.00	0.00	0.00
Z-score	0.81	0.77	0.69	0.73	0.78	0.85	0.88	0.85	0.62	0.62

References

1. Law CJ. 2019 Solitary meat-eaters: solitary, carnivorous carnivorans exhibit the highest degree of sexual size dimorphism. *Sci Rep-uk* **9**, 15344. (doi:10.1038/s41598-019-51943-x)

2. Polly PD, Lawing AM, Fabre A-C, Goswami A. 2013 Phylogenetic principal components analysis and geometric morphometrics. *Hystrix, the Italian Journal of Mammalogy* **24**, 33–41.

3. Greaves WS. 2012 The Mammalian Jaw. , 3–25. (doi:10.1017/cbo9781139060851.003)

4. Davis DD. 1964 *The giant panda: a morphological study of evolutionary mechanisms*. Fieldiana (Zoology Memoirs). (doi:10.5962/bhl.title.5133)

5. Samuels JX, Meachen JA, Sakai SA. 2013 Postcranial morphology and the locomotor habits of living and extinct carnivorans. *J Morpho* **274**, 121–146. (doi:10.1002/jmor.20077)

6. Jones KE, Dickson BV, Angielczyk KD, Pierce SE. 2021 Adaptive landscapes challenge the "lateral-to-sagittal" paradigm for mammalian vertebral evolution. *Curr. Biol.* **31**, 1883-1892.e7. (doi:10.1016/j.cub.2021.02.009)

7. Jones KE, Gonzalez S, Angielczyk KD, Pierce SE. 2020 Regionalization of the axial skeleton predates functional adaptation in the forerunners of mammals. *Nat Ecol Evol* **4**, 470–478. (doi:10.1038/s41559-020-1094-9)

8. Boszczyk BM, Boszczyk AA, Putz R. 2001 Comparative and functional anatomy of the mammalian lumbar spine. *Anatomical Rec* **264**, 157–168. (doi:10.1002/ar.1156)

9. Law CJ, Young C, Mehta RS. 2016 Ontogenetic scaling of theoretical bite force in southern sea otters (Enhydra lutris nereis). *Physiol Biochem Zool* **89**, 347–363. (doi:10.1086/688313)

10. Throckmorton GS, Dean JS. 1994 The relationship between jaw-muscle mechanical advantage and activity levels during isometric bites in humans. *Arch. Oral Biol.* **39**, 429–437. (doi:10.1016/0003-9969(94)90174-0)

11. Santana SE, Grosse IR, Dumont ER. 2012 Dietary hardness, loading behavior, and the evolution of skull form in bats. *Evolution* **66**, 2587–2598. (doi:10.1111/j.1558-5646.2012.01615.x)

12. Smith JM, Savage RJG. 1956 Some locomotory adaptations in mammals. *J Linn Soc Lond Zoology* **42**, 603–622. (doi:10.1111/j.1096-3642.1956.tb02220.x)

13. Gasc J-P. 2001 Comparative aspects of gait, scaling and mechanics in mammals. *Comp. Biochem. Physiol. Part A: Mol. Integr. Physiol.* **131**, 121–133. (doi:10.1016/s1095-6433(01)00457-3)

14. Polly PD. 2007 Limbs in mammalian evolution. In *Fins into Limbs Evolution, Development, and Transformation* (ed BK Hall), pp. 245–268. Fins into Limbs Evolution, Development, and Transformation.

15. Schmidt M, Fischer MS. 2009 Morphological integration in mammalian limb proportions: dissociation between function and development. *Evolution* **63**, 749–766. (doi:10.1111/j.1558-5646.2008.00583.x)

16. Fischer MS, Schilling N, Schmidt M, Haarhaus D, Witte H. 2002 Basic limb kinematics of small therian mammals. *J. Exp. Biol.* **205**, 1315–1338. (doi:10.1242/jeb.205.9.1315)

17. Strang KT, Steudel K. 1990 Explaining the scaling of transport costs: the role of stride frequency and stride length. *J. Zoo□l.* **221**, 343–358. (doi:10.1111/j.1469-7998.1990.tb04006.x)

18. Kram R, Taylor CR. 1990 Energetics of running: a new perspective. *Nature* **346**, 265–267. (doi:10.1038/346265a0)

19. Garland T, Janis CM. 1993 Does metatarsal/femur ratio predict maximal running speed in cursorial mammals? *J. Zoo□l.* **229**, 133–151. (doi:10.1111/j.1469-7998.1993.tb02626.x)

20. Kilbourne BM, Hoffman LC. 2013 Scale Effects between Body Size and Limb Design in Quadrupedal Mammals. *PLoS ONE* **8**, e78392. (doi:10.1371/journal.pone.0078392)

21. Pontzer H. 2007 Effective limb length and the scaling of locomotor cost in terrestrial animals. *J. Exp. Biol.* **210**, 1752–1761. (doi:10.1242/jeb.002246)

22. Pontzer H. 2007 Predicting the energy cost of terrestrial locomotion: a test of the LiMb model in humans and quadrupeds. *J. Exp. Biol.* **210**, 484–494. (doi:10.1242/jeb.02662)

23. Christiansen P. 2002 Locomotion in terrestrial mammals: the influence of body mass, limb length and bone proportions on speed. *Zoo□l. J. Linn. Soc.* **136**, 685–714. (doi:10.1046/j.1096-3642.2002.00041.x)

24. Samuels JX, Valkenburgh BV. 2008 Skeletal indicators of locomotor adaptations in living and extinct rodents. *J Morpho* **269**, 1387–1411. (doi:10.1002/jmor.10662)

25. Kemp TJ, Bachus KN, Nairn JA, Carrier DR. 2005 Functional trade-offs in the limb bones of dogs selected for running versus fighting. *J. Exp. Biol.* **208**, 3475–3482. (doi:10.1242/jeb.01814)

26. Kilbourne BM. 2017 Selective regimes and functional anatomy in the mustelid forelimb: Diversification toward specializations for climbing, digging, and swimming. *Ecol Evol* **66**, 2369–12. (doi:10.1002/ece3.3407)

27. Rickman J, Burtner AE, Linden TJ, Santana SE, Law CJ. 2023 Size And Locomotor Ecology Have Differing Effects on the External and Internal Morphologies of Squirrel (Rodentia: Sciuridae) Limb Bones. *Integr. Org. Biol.* **5**, obad017. (doi:10.1093/iob/obad017)

28. Hildebrand M. 1985 Digging of Quadrupeds. In *Functional Vertebrate Morphology* (eds M Hildebrand, DM Bramble, KF Liem, DB Wake), pp. 89–109. Cambridge, MA: Harvard University Press. (doi:10.4159/harvard.9780674184404.c6)

29. Lessa EP, Stein BR. 1992 Morphological constraints in the digging apparatus of pocket gophers (Mammalia: Geomyidae). *Biol J Linn Soc* **47**, 439–453. (doi:10.1111/j.1095-8312.1992.tb00678.x)

30. Lagaria A, Youlatos D. 2006 ANATOMICAL CORRELATES TO SCRATCH DIGGING IN THE FORELIMB OF EUROPEAN GROUND SQUIRRELS (SPERMOPHILUS CITELLUS). *J Mammal* **87**, 563–570. (doi:10.1644/05-mamm-a-251r1.1)

31. Rose J, Moore A, Russell A, Butcher M. 2014 Functional osteology of the forelimb digging apparatus of badgers. *J. Mammal.* **95**, 543–558. (doi:10.1644/13-mamm-a-174)

32. Martín-Serra A, Pérez-Ramos A, Pastor FJ, Velasco D, Figueirido B. 2021 Phenotypic integration in the carnivoran backbone and the evolution of functional differentiation in metameric structures. *Evolution Letters* , 1–14. (doi:10.1002/evl3.224)

33. Law CJ. 2021 Ecological drivers of carnivoran body shape evolution. *Am Nat* **198**, 406–420. (doi:10.5061/dryad.pg4f4qrpm)

34. Law CJ, Blackwell EA, Curtis AA, Dickinson E, Hartstone□Rose A, Santana SE. 2022 Decoupled evolution of the cranium and mandible in carnivoran mammals. *Evolution* **76**, 2959–2974. (doi:10.1111/evo.14578)

35. Dickson BV, Clack JA, Smithson TR, Pierce SE. 2021 Functional adaptive landscapes predict terrestrial capacity at the origin of limbs. *Nature* **589**, 242–245. (doi:10.1038/s41586-020-2974-5)

36. Dickson BV, Pierce SE. 2019 Functional performance of turtle humerus shape across an ecological adaptive landscape. *Evolution* **73**, 1265–1277. (doi:10.1111/evo.13747)

37. Polly PD, Stayton CT, Dumont ER, Pierce SE, Rayfield EJ, Angielczyk KD. 2016 Combining Geometric Morphometrics and Finite Element Analysis with Evolutionary Modeling: Towards a Synthesis. *J Vertebr Paleontol* **36**, e1111225. (doi:10.1080/02724634.2016.1111225)